ARMY RESEARCH LABORATORY

ARL

Ultrahigh-Strength Magnesium Alloys for the Future Force: A Final Report on the 5-Year Mission Program, 2009–2013

by Vincent Hammond, Suveen Mathaudhu, Kevin Doherty, Shawn Walsh, Lionel Vargas, Brian Placzankis, Joseph Labukas, Marc Pepi, Matt Trexler, Blake Barnett, Tyrone Jones, and Laszlo Kecskes

ARL-TR-6788   **January 2014**

NOTICES

Disclaimers

Army Research Laboratory

Aberdeen Proving Ground, MD 21005-5069

ARL-TR-6788   **January 2014**

Ultrahigh-Strength Magnesium Alloys for the Future Force: A Final Report on the 5-Year Mission Program, 2009–2013

Vincent Hammond, Suveen Mathaudhu, Kevin Doherty, Shawn Walsh, Lionel Vargas, Brian Placzankis, Joseph Labukas, Marc Pepi, Matt Trexler, Blake Barnett, Tyrone Jones, and Laszlo Kecskes

Weapons and Materials Research Directorate, ARL

REPORT DOCUMENTATION PAGE			*Form Approved* *OMB No. 0704-0188*

Public reporting burden for this collection of information is estimated to average 1 hour per response, including the time for reviewing instructions, searching existing data sources, gathering and maintaining the data needed, and completing and reviewing the collection information. Send comments regarding this burden estimate or any other aspect of this collection of information, including suggestions for reducing the burden, to Department of Defense, Washington Headquarters Services, Directorate for Information Operations and Reports (0704-0188), 1215 Jefferson Davis Highway, Suite 1204, Arlington, VA 22202-4302. Respondents should be aware that notwithstanding any other provision of law, no person shall be subject to any penalty for failing to comply with a collection of information if it does not display a currently valid OMB control number.
PLEASE DO NOT RETURN YOUR FORM TO THE ABOVE ADDRESS.

1. REPORT DATE *(DD-MM-YYYY)* January 2014	2. REPORT TYPE Final	3. DATES COVERED (From - To) October 2008–September 2013

4. TITLE AND SUBTITLE Ultrahigh-Strength Magnesium Alloys for the Future Force: A Final Report on the 5-Year Mission Program, 2009–2013	5a. CONTRACT NUMBER
	5b. GRANT NUMBER
	5c. PROGRAM ELEMENT NUMBER
6. AUTHOR(S) Vincent Hammond, Suveen Mathaudhu, Kevin Doherty, Shawn Walsh, Lionel Vargas, Brian Placzankis, Joseph Labukas, Marc Pepi, Matt Trexler, Blake Barnett, Tyrone Jones, and Laszlo Kecskes	5d. PROJECT NUMBER
	5e. TASK NUMBER
	5f. WORK UNIT NUMBER

7. PERFORMING ORGANIZATION NAME(S) AND ADDRESS(ES) U.S. Army Research Laboratory ATTN: RDRL-WMM-F Aberdeen Proving Ground, MD 21005-5069	8. PERFORMING ORGANIZATION REPORT NUMBER ARL-TR-6788

9. SPONSORING/MONITORING AGENCY NAME(S) AND ADDRESS(ES)	10. SPONSOR/MONITOR'S ACRONYM(S)
	11. SPONSOR/MONITOR'S REPORT NUMBER(S)

12. DISTRIBUTION/AVAILABILITY STATEMENT

Approved for public release; distribution is unlimited.

13. SUPPLEMENTARY NOTES

14. ABSTRACT

Although highly desired because of their low density, magnesium (Mg) alloys have long been passed over for military applications in favor of aluminum alloys due to their low strength and poor corrosion resistance. However, continued advances in Mg alloy development have resulted in a renewed interest within the U.S. Army regarding their use in both structural and protection applications. As a result, in 2009, the U.S. Army Research Laboratory initiated a 5-year research effort to understand the fundamental scientific mechanisms governing the mechanical properties and corrosion performance behavior of Mg alloys. This report details the results of in-house and collaborative efforts in areas such as enhancing mechanical properties through grain refinement and minimizing texture, improving corrosion performance through coatings and elemental additions, and computational modeling to identify underlying mechanisms that govern ductility and processing pathways. The knowledge and insight gained from this multifaceted approach has advanced the state of the art for Mg alloys, thereby increasing their potential insertion into Army systems.

15. SUBJECT TERMS

Mg, ECAE, corrosion, personnel protection, ballistics

16. SECURITY CLASSIFICATION OF:			17. LIMITATION OF ABSTRACT	18. NUMBER OF PAGES	19a. NAME OF RESPONSIBLE PERSON Vincent Hammond
a. REPORT Unclassified	b. ABSTRACT Unclassified	c. THIS PAGE Unclassified	UU	76	19b. TELEPHONE NUMBER *(Include area code)* 410-306-4961

Contents

List of Figures

v

vii

List of Tables

1. Introduction

In contrast to conventional thought, magnesium (Mg) alloys have been widely used in military systems prior to current times. Indeed, clear correlations can be observed between recent times of conflict and an increase in U.S. Mg production (*1*). The impetus for the rapid escalation of use was the need to utilize all available resources during the time of war. In each conflict, Mg alloys provided a means for meeting specialized needs in military applications.

However, despite their widespread use in wartime, the use of Mg alloys dropped precipitously after the end of each conflict. Factors commonly provided for this were poor tensile properties and corrosion resistance, as well as a perceived flammability concern. Additional factors that served to hinder the insertion of Mg alloys into widescale usage were poor formability at low temperatures (lower than 250 °C), a higher cost relative to aluminum (Al) alloys, and poor creep performance. As a result, it is not surprising that Al alloys were developed and adopted at a far faster pace than Mg-based alloys.

In large part because of an ever-increasing need for lightweight structures, Mg alloys became the focus of renewed research starting in the late 1990s. Initially, these efforts resulted in advances in the area of alloy design and protective coatings that helped to alleviate corrosion concerns. In addition, processing methods such as equal channel angular extrusion (ECAE) and high-pressure torsion were shown to yield ultrafine-grained (UFG) materials with significant strength improvements. Finally, next-generation alloys that contained a variety of rare earth elements were discovered and rapidly developed, improving material strengths and corrosion resistance.

As a result of the rapid progress in Mg alloy development, there has been a renewed interest in their potential for use in defense-related applications. Not surprisingly, areas of particular interest to the U.S. Army are the use of these alloys in both structural and ballistic applications to achieve significant lightening of vehicular platforms. Based on this strong interest, the U.S. Army Research Laboratory (ARL) initiated a 5-year study in 2009 to develop ultrahigh-strength Mg alloys suitable for Army-related applications. This report presents the findings of this study and casts a vision for the future of Mg research at ARL.

2. Historical Perspective

First identified by Sir Humphrey Davy in 1808, elemental Mg is the eighth most abundant element in the Earth's crust and the third most dissolved element in seawater. Indeed, it has been estimated that a cubic mile of seawater contains 6 million tons of Mg metal (*2*). Although first

produced by electrolysis in 1833 by Michael Faraday, the German chemist Robert Bunsen is credited with the first commercial production of Mg in 1852. This early involvement resulted in German scientists being the leading experts in the initial stages of Mg production and metallurgical studies. More recently, China has assumed the lead in the research and development of Mg alloys due to its dominant position as the world's leading producer (greater than 80%) of elemental Mg.

On first inspection, Mg has several properties that would suggest widespread use in a variety of engineering applications. In addition to being the lowest-density structural metal, Mg has high specific properties, good electrical and thermal conductivity, and a high damping capacity. However, despite their many attractive properties, concerns regarding corrosion, flammability, and mechanical properties have caused the use of Mg alloys to lag far behind other lightweight metals such as Al and titanium. Indeed, the primary use of Mg has historically been as an elemental addition to Al-based alloys. As a result, in 2009, Al production was approximately 30 million tons per year while Mg was only 0.8 million tons per year (*2*).

However, over the past 20–30 years, Mg alloys have become accepted as viable engineering materials. One factor contributing to the turnaround was a consistent, albeit small, research community that managed to successfully address the aforementioned concerns by developing an understanding of which elements are beneficial or harmful to Mg. This knowledge has led to new alloy families as well as guidance concerning the influence of type and level of impurities on corrosion resistance. Secondly, the massive growth in Mg production occurring in China due to the widespread use of the Pidgeon process has driven the cost of Mg down to the point that it is essentially the same as that of Al. Finally, there is also that realization in many sectors that desired weight savings, and concomitant performance improvements, can be achieved only through the use of Mg alloys.

One industry that is seeking to expand the use of Mg is automotive manufacturing. Data from 2004 indicate that the use of Mg in the automotive industry had grown by 10%−15% per year over the previous 15 years (*3*). Despite this impressive growth, the use of Mg amounted to an average of only 10–12 lb—out of approximately 3360 lb—in a standard passenger vehicle. In order to accelerate the use of Mg in the automotive industry, leading experts in automotive materials met at the U.S. Council for Automotive Research in 2004. Their observations and recommended actions were published in a report entitled "Magnesium Vision 2020: A North American Automotive Strategic Vision for Magnesium" (*3*). Problem areas identified in the report included cost and quality of high-pressure die cast parts, fastening/corrosion, and a limited infrastructure that could not develop and market competitive solutions.

Since then, additional workshops have been held to discuss potential applications for Mg alloys in the automotive industry. In March 2011, the U.S. Department of Energy hosted the 2011 Advanced Materials Roadmapping Workshop in Detroit, which identified current trends and future projections for achieving weight savings in both light-duty (car) and heavy-duty (truck)

systems. Among metallic materials, Mg alloys were again broadly discussed as materials of interest. In general, there was a positive attitude regarding the use of Mg, although some problem areas to be addressed were identified. Indeed, note that many of the previously identified concerns, e.g., corrosion, multimaterial joining, and high-temperature strength properties, appeared on the list generated at this workshop as well. One new area that was identified by several panel members was the need for improved predictive capabilities in both alloy design/processing and mechanical performance (failure).

In May 2011, the National Science Foundation hosted a workshop on Mg in Washington, DC, that brought together the leading academic and industrial researchers to discuss the current state of Mg research. Although not specific to automotive-related applications, many of the issues identified are relevant to this industry. For example, the lack of acceptable high-temperature properties (e.g., strength and creep) was noted as a limiting factor for the use of Mg alloys in engine components. Another significant factor cited was the lack of advances in the processing area, whether in a predictive capability or in actual casting and/or wrought process developments. As an example, it was noted that there has been no new casting research in over 10 years in Europe. As a result, the near-term potential for the further introduction of Mg parts is limited, as there is only one processing method, high-pressure die casting, that is capable of producing Mg components with the necessary properties.

Although there is appreciable interest in Mg alloys in the automotive industry, significant hurdles remain to be overcome for Mg alloys to be fully utilized. Provided these hurdles can be successfully addressed, there is every reason to expect future automotive designs to fully capitalize on the benefits offered by this material.

In contrast to the automotive industry, Mg and its alloys have been used in numerous military applications, primarily during times of conflict when the desperate need for the material outweighed its shortcomings. For example, during World War I, primary usage was in tracer rounds and incendiary flares. By World War II, the potential for lightening was recognized and Mg alloys were widely used in a broad range of aerospace applications, such as aircraft fuselages, wing skins, structural frame members, and decking/flooring. During the Korean and Vietnam eras, Mg use expanded to include components in helicopters, missiles, and a variety of land vehicles.

Although Mg alloys have managed to find usage in a broad range of structural applications, their use in ballistic protection has not been as easily accepted. Initial evaluation of "Dowmetal," a refined Mg alloy containing Al and manganese, was conducted during World War II. However, these materials were found to have lower perforation resistance than either face-hardened steel or age-hardenable Al alloys. As a result, after World War II, advanced steels and Al alloys became the metals of choice for use in armor applications. It wasn't until slightly less than 10 years ago that a Mg alloy, AZ31B, was evaluated for its ballistic performance.

AZ31B is a wrought alloy that contains approximately 3 w% Al and 1 w% zinc (Zn), and is available as fully or partially annealed plate after hot rolling. In a study performed at ARL in 2007, AZ31B was measured against a range of threats (0.30-cal. armor-piercing APM2, 0.50-cal. APM2, 0.22-cal. fragment-simulating projectile [FSP], 0.50-cal. FSP, and 20-mm FSP) (*4*). When compared with historical results for Al alloy 5083, AZ31B was found to be nearly equivalent on an areal density basis for all threats except the 20-mm FSP. Surprisingly, based on areal density, AZ31B outperformed rolled homogenous armor (RHA) steel against 0.22-cal. and 20-mm FSP while matching it against the 0.50-cal. APM2. AZ31B performed to a lesser degree than RHA steel against 0.30-cal APM2 and 0.50-cal. FSP. However, these results are diminished somewhat by the fact that the thickness of the Mg plate was approximately four times that of the steel plate and 1.5 times that of Al alloy 5083. That said, these results are noteworthy because AZ31B is a general-purpose engineering alloy that was not optimized for ballistic performance.

The progressive development of advanced Mg alloys with improved performance resulted in a renewed interest by the Department of Defense (DOD). Indeed, an international workshop on advanced Mg alloys held at The Johns Hopkins University in May 2007 concluded that Mg alloys have potential for various Army applications in lightweight structures and armor systems and may have potential strategic importance to the nation (*5*). As a result, the workshop participants offered the general recommendation that the Army lead a DOD-sponsored effort to rapidly establish a research and development program focused on fundamental performance issues such as deformation mechanisms, corrosion, texture evolution, and high strain rate behavior. Specifically, panel members identified the need to develop alloys in the near term with yield strengths of approximately 350 MPa with an ultimate goal of at least 500 MPa while maintaining a ductility of at least 10%. It was realized that these goals would necessitate the development of processing methods that yield fine, randomly oriented grains that would minimize texture and anisotropy. Of the processing methodologies, severe plastic deformation, specifically ECAE, was identified as one of many viable methods that had the potential for producing such microstructures, but much work remained to develop appropriate processing paths. The importance of computational modeling, whether for alloy design or predicting properties and/or performance, was also highlighted. Finally, it was recognized that work was needed to break down misperceptions regarding the flammability of modern Mg alloys.

3. Development of the ARL Program

In response to the findings detailed in the previous section, a 1-year seed effort was undertaken by ARL in 2008 to evaluate selected severe plastic deformation techniques based on their ability to produce fine-grained Mg alloys. The objective was to identify the processing method(s) that provided the most promising pathway for obtaining the desired combination of microstructure,

texture, and mechanical performance. Relationships between texture and property anisotropy would also be determined. The intention of the effort would be to establish a technology roadmap for obtaining samples suitable for determining the effects of UFG size on ballistic performance in Mg alloys. A review of available severe plastic deformation methods resulted in a selection of the following methods and university partners: alternate biaxial reverse corrugation (ABRC), University of Michigan; high-pressure torsion (HPT), North Carolina State University (NCSU); and ECAE, Texas A&M University.

3.1 Alternate Biaxial Reverse Corrugation (ABRC), University of Michigan

In this method, a sample billet is subjected to the desired amount of true strain by being corrugated between sine wave dies using a series of successive rotations followed by flattening. Simultaneously, the material is reduced in thickness until the desired final value is achieved. Thus, the method offers the ability to achieve a broad range of final thickness values in the processed billet. Figure 1 shows a schematic of the process and a picture of a representative sample.
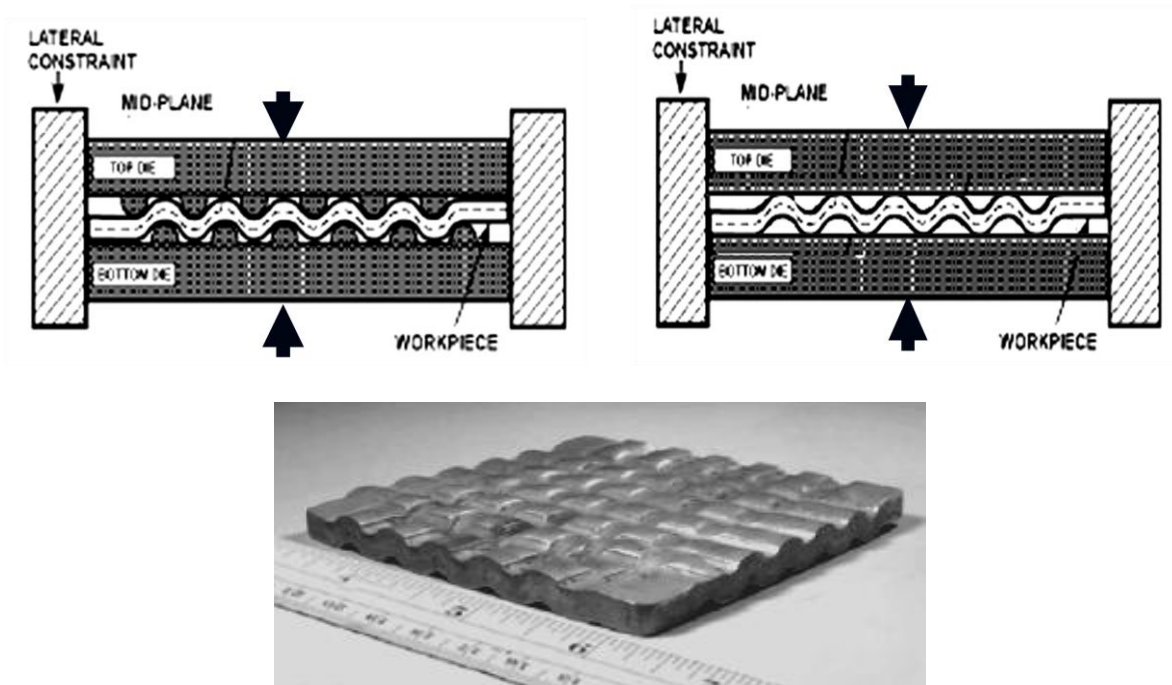
Figure 1. Schematic representation and representative plate specimen associated with the ABRC process.

As part of this effort, ABRC was used to produce a ZK60 (Mg – 5.5 w% Zn – 0.45w% Zr [zirconium]) alloy with a refined grain size of approximately 1 μm. ABRC was conducted on representative samples at a temperature range of 320–350 °C or progressively reducing the temperature from 250 to 150 °C during processing. In the case of one sample, ABRC was followed by hot rolling at 250 °C and pressing at 150 °C. Stress-strain curves for the processed

samples are shown in figure 2 with tabulated data given in table 1. For comparative purposes, the as-cast properties of ZK60 are a yield strength of 155 MPa, an ultimate tensile strength of 185 MPa, and an elongation on the order of 5%.
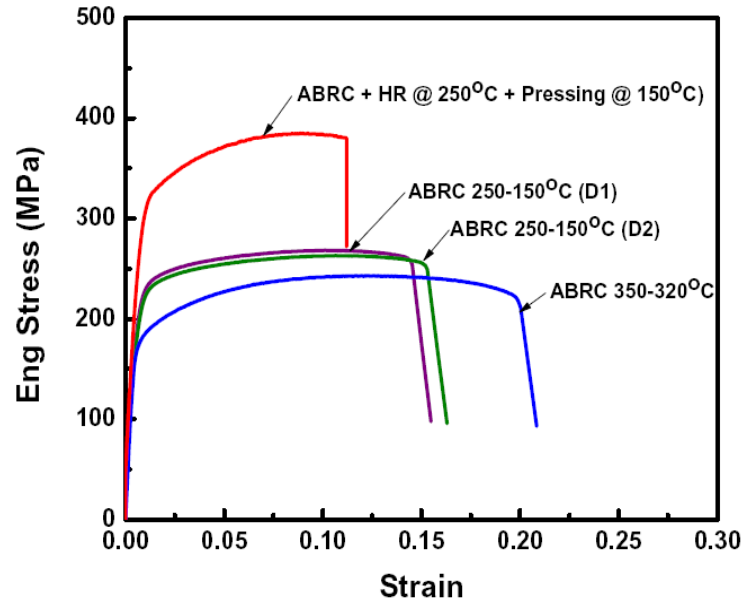
Figure 2. Stress-strain curves obtained from ZK60
samples processed using ABRC.

Table 1. Thickness, grain size, and mechanical properties obtained from plates ABRC processed using the indicated conditions.

Material	Thickness (mm)	Grain Size (µm)	Tensile Yield Strength (MPa)	Ultimate Tensile Strength (MPa)	ε_t (%)
ABRC at 350–320 °C	3	2.5	175	242	20.8
ABRC at 250–150 °C (D1)	1.5	1.2	210	263	15.5
ABRC at 250–150 °C (D2)	1.5	1.2	205	269	16
ABRC + HR at 250 °C + HP at 150 °C	0.75	—	320	386	11

3.2   High-Pressure Torsion (HPT), North Carolina State University

The second severe plastic deformation process evaluated was HPT. In this method, an extremely high hydrostatic pressure is applied in compression to a small sample located between two anvils (see figure 3). While the load is applied, one of the anvils is rotated, resulting in the torsion of the sample. Because of the high hydrostatic compression, the strain to fracture for the sample is increased to an essentially infinite value. Thus, with continued rotation, the desired amount of shear strain can be applied to the sample, during which significant grain refinement can be achieved. Drawbacks to the method are that sample size is typically restricted to a 10- to 22-mm diameter and that grain size and property variations exist across the diameter due to the gradient in torsional strain from the center to edge of the sample. An example of the microhardness

variation across the sample diameter for alloy ZK60 is shown in figure 4. Using the approximation that tensile yield strength is approximately one-third of the microhardness, the yield strength for the ZK60 sample ranges from approximately 300 MPa at the center to 425 MPa at the edge.
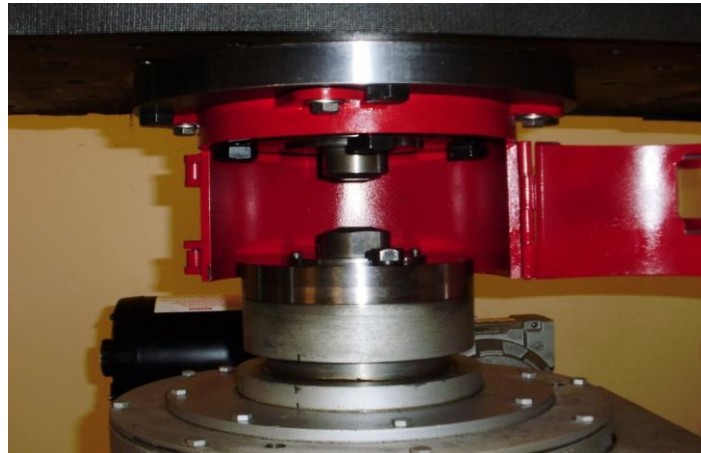
Figure 3. Picture of the HPT processing chamber as well as 10-mm-diameter ZK60 sample processed for six turns under 1-GPa pressure.
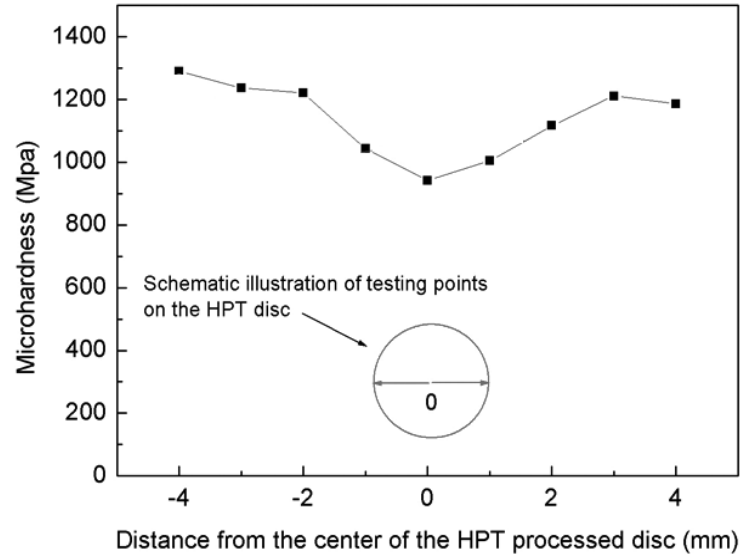
Figure 4. Variation in microhardness across the diameter
of a ZK60 sample produced via HPT.

In addition, $MgZn_1Y_2$ alloy powders produced by mechanical alloying were consolidated through the use of HPT. This alloy was first developed by Inoue et al. (*6*) and exhibited a yield strength of approximately 610 MPa with 5% elongation. The high strength was attributed to a fine grain size and the presence of a long-period stacking-ordered structure consisting of a solid solution of yttrium (Y) and Zn in a Mg matrix where these atoms are periodically located in the Mg basal planes. Measurements from the NCSU powders indicated an average grain size of 25 nm, with an average hardness in the as-processed powder and consolidated sample of approximately 1.65 GPa and 1.90 GPa or an anticipated tensile strength of 550 and 630 MPa, respectively (see figure 5).
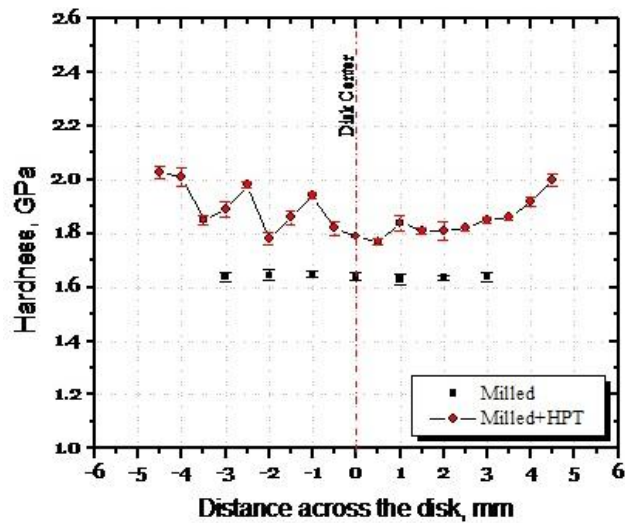
Figure 5. Hardness values across sample diameter
for $MgZn_1Y_2$ milled powder as well as
HPT-processed disc.

3.3 Equal Channel Angular Extrusion (ECAE), Texas A&M University

The final technique evaluated during the initial effort was ECAE, in which strain is imposed on a sample billet by forcing the work piece around a sharp bend in an extrusion die. As the cross section of the extrusion channel is the same before and after the bend, there is essentially no change in the dimensions of the work piece. Thus, it is relatively straightforward to impose the desired level of strain on the sample by simply performing multiple extrusion passes. This is in sharp contrast to more well-known methods such as rolling, forging, or extrusion, which can produce materials with a fine-grain structure but do so by dimensional reduction in at least one direction (thickness). As a result, ECAE has an almost unequalled potential for producing rods and/or plates with the desired degree of work hardening and microstructural refinement. The ECAE effort focused on fundamental studies designed to identify correlations between processing conditions, microstructural development, and mechanical properties for the AZ31B Mg alloy. As a result, the majority of experimental studies were done using a single temperature with a limited number of route variations and passes.

The development of a strong texture and the resulting anisotropy in mechanical properties are well-known facts associated with Mg. Indeed, an early study on AZ31B showed that the highly anisotropic response and hardening behavior can be attributed to the texture formed during ECAE processing (*7*). However, as this work only considered one starting sample orientation, a limited study evaluated the influence of sample orientation (basal poles parallel to the extrusion or flow direction) after one pass (route A) at 200 °C (*8*). These experiments indicated that the initial grain orientation significantly affected the evolution of texture and grain morphology. Indeed, although dynamic recrystallization took place in both samples, it was more prevalent in the sample in which the basal poles were parallel to the extrusion direction. In addition, a reduction in the amount of flow anisotropy was observed when there was a larger degree of random basal plane distribution.

This work was extended to investigate the influence of processing route on AZ31B with a single starting texture (*9*). In this case, samples were processed at 200 °C up to a total of four passes following routes A, C, E, or B_c. Not surprisingly, the degree of microstructural uniformity increased with the number of passes, with the finest microstructure observed in samples processed using route B_c. Mechanical testing indicated that samples with similar textures had similar responses in tension and compression. Finally, it was shown that a viscoplastic self-consistent (VPSC) crystal plasticity model was capable of predicting the evolution of texture observed in the samples.

In a similar study examining the influence of texture and grain size on anisotropy in ECAE-processed AZ31B, it was determined that the grain size effect was rather weak in most orientations (*10*). Yet it was observed that mechanical anisotropy actually increased with texture strength. That is, the flow anisotropy is lowest in samples that had the highest amount of

randomly oriented basal planes. This observation was critical, as it supported the theory that a Mg alloy with a minimal amount of anisotropy is possible, provided that the final texture is highly randomized.

3.4 Summary

A trio of severe plastic deformation techniques was evaluated over a 1-year period to determine their suitability for producing Mg alloys with a fine-grained uniform microstructure. Each of the respective methods has their own significant advantage. For example, ABRC offers the possibility of producing thin sheets with a refined grain size and enhanced mechanical properties. The use of HPT allows one to impose an almost endless amount of strain on a material, thereby achieving a significant amount of strengthening through a highly refined microstructure. However, both of these methods are limited in the sample size that can realistically be produced. As a result, of the three examined in detail, ECAE offered the most promising approach for microstructural and property enhancement, as well as the greatest potential for upscaling to industrially relevant sizes.

4. ARL 5-Year Plan

Following the success of this 1-year effort, a 5-year mission effort was developed to further explore the processing and performance of UFGed Mg alloys. Specifically, the ability to produce ultrahigh-strength Mg alloys with significantly improved properties using ECAE would be determined. Initially, sample size would be on the order of 3/4-in square bars (up to 8 in length), with the intent to upscale by the end of the project to 12- × 12- × 1-in plate samples. Although the bars could be used to correlate processing conditions to microstructural and property development, the large plates would enable ballistic testing against an array of representative threats. In addition, complimentary efforts would also be undertaken to evaluate alternative processing and joining methods, corrosion performance, and other topic areas relevant to the U.S. Army.

4.1 ECAE Process Development

Earlier efforts clearly indicated that ECAE offered the greatest potential for achieving UFGed Mg for numerous Army applications. As a result, the decision was made to focus on developing a detailed understanding and ability to produce UFGed Mg alloys using ECAE. Toward that end, a cooperative agreement was established with Texas A&M University to further advance the knowledge and understanding of ECAE processing of Mg and its alloys. Specific areas of interest were the relationships between processing conditions and resulting development of crystallographic texture, microstructure, and mechanical properties. An effort was also undertaken to predict microstructural evolution and texture using VPSC models.

During the 1-year initial effort, one factor that was observed to adversely affect the final grain size was dynamic recrystallization, a phenomenon that can occur in Mg alloys for temperatures as low as approximately 150 °C (see figure 6). In an effort to minimize recrystallization, processing routes were developed that started at 200 °C for the initial homogenization of the grain size but finished at temperatures below 200 °C in order to "freeze in" the finer grain size achieved during earlier passes. These routes, denoted as hybrid routes, typically involved multiple passes at one temperature followed by a sample rotation and continued processing at a reduced temperature. In addition to the finer grain size, such a complex route history also showed promise for reducing anisotropy by strain hardening basal slip, as well as suppressing twinning and shear localization. Shown in figure 7 are optical and scanning electron micrographs depicting the progressive reduction in final grain size achieved with the temperature reduction method.
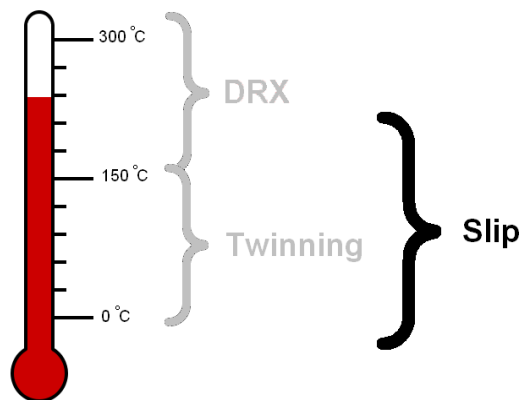
Figure 6. Temperature range associated with
various mechanisms in Mg alloys.
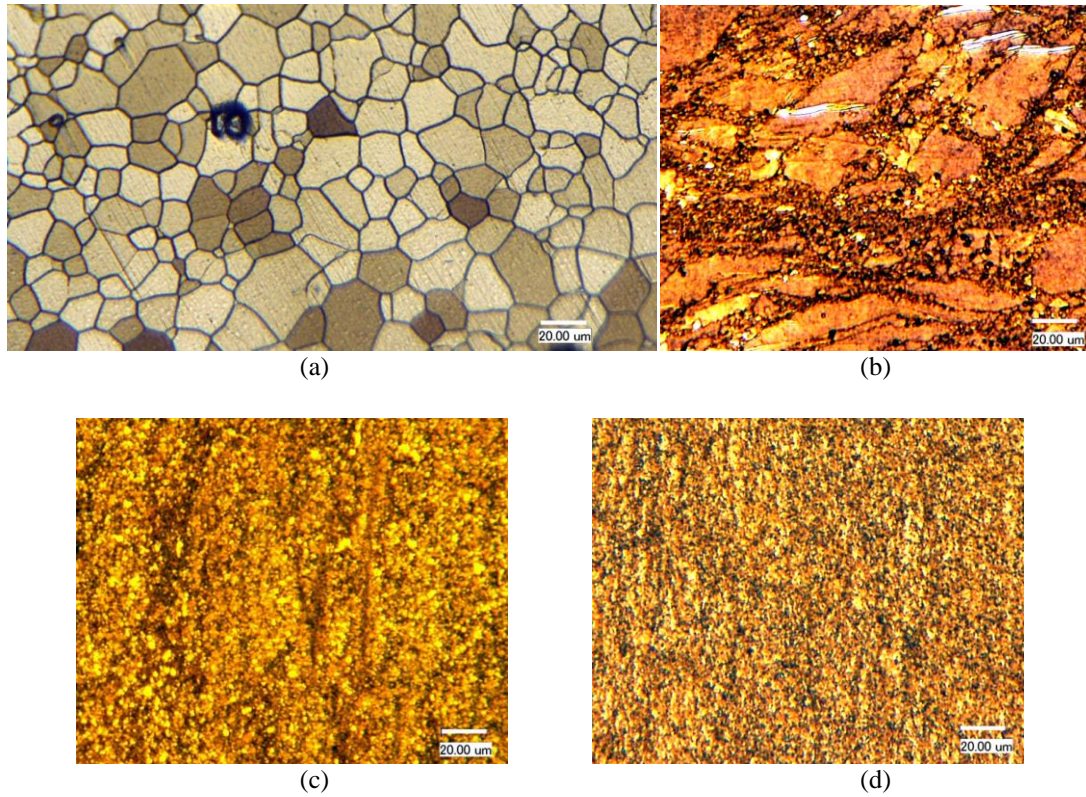
Figure 7. Microstructural development resulting from the following conditions: (a) AZ31B, annealed 12 h/350 °C, 5- to 20-µm grain size; (b) 1A at 200 °C, 1- to 30-µm grain size; (c) 2A at 200 °C, 2A at 150 °C, 1A at 125 °C, 1- to 4-µm grain size; and (d) 4A at 200 °C, 2A at 150 °C, 1A at 125 °C, 0.5- to 2-µm grain size.

Concurrent with the development of processing routes, the ability of the VPSC model to predict the final state of the processed alloy was also being developed. In VPSC models, each grain is treated as an ellipsoidal viscoplastic inclusion embedded in and interacting with an anisotropic homogenous medium. By taking the average of the stress and strain tensors for all grains, it is possible to calculate corresponding components in the stress and strain tensor for the entire medium. Using the single crystal properties of Mg, as well as the initial texture and deformation path as input, the model is able to predict the texture, deformation activities, and mechanical response for one ECAE processing route. The calculated properties can then be used for input into the next processing route until the entire processing cycle is completed. For example, figure 8 compares predicted and measured texture development in AZ31B alloy subjected to the indicated ECAE processing schedule.
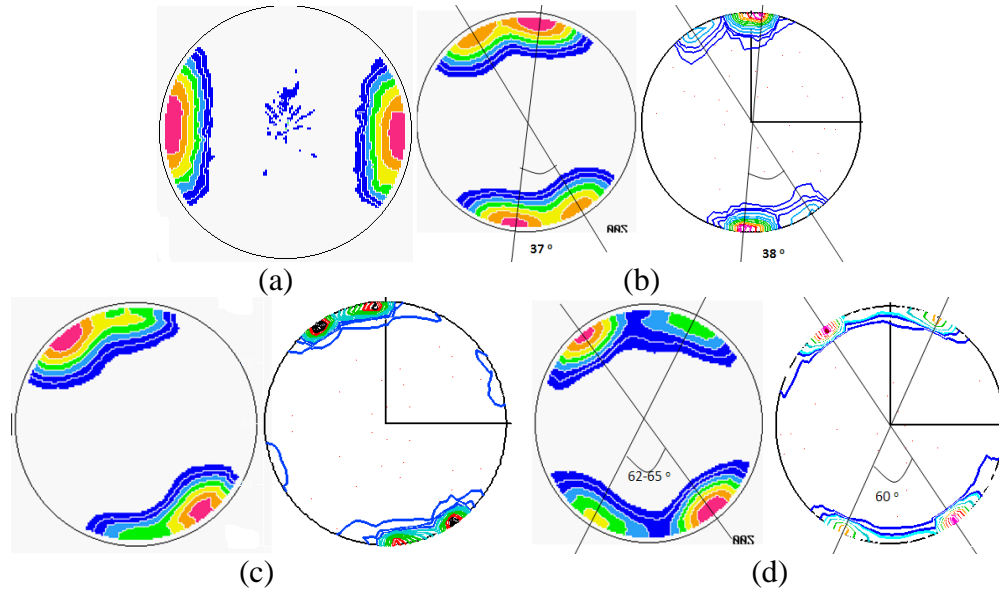
Figure 8. Experimental vs. predicted texture development for AZ31B: (a) starting texture;
(b) route 1A; (c) route 2A, 180° rotation about extrusion direction (ED) 2A; and
(d) 2A, 180° rotation about ED, plus 2A, 180° rotation about ED, plus 1A.

In addition to predicting the final texture, mechanical performance, and grain morphology and structure (size, shape), VPSC models can also provide insight into the deformation mechanisms that are active during a given processing routine. For example, figure 9 illustrates the texture evolution and relative activity of deformation systems in AZ31B subjected to ECAE processing in which the lower temperature pass has been changed from route A to B_c. The differences in the relative activities in (c) and (d) suggest that the nonuniform microstructure in the latter sample could be a consequence of prismatic slip. Shown in figure 10 is the predicted compression response of Zr after one ECAE pass. Thus, it is clear that through the use of the VPSC model one can design a processing route that provides the desired level of texture and/or flow anisotropy.

(a)

(b)

(c)

(d)
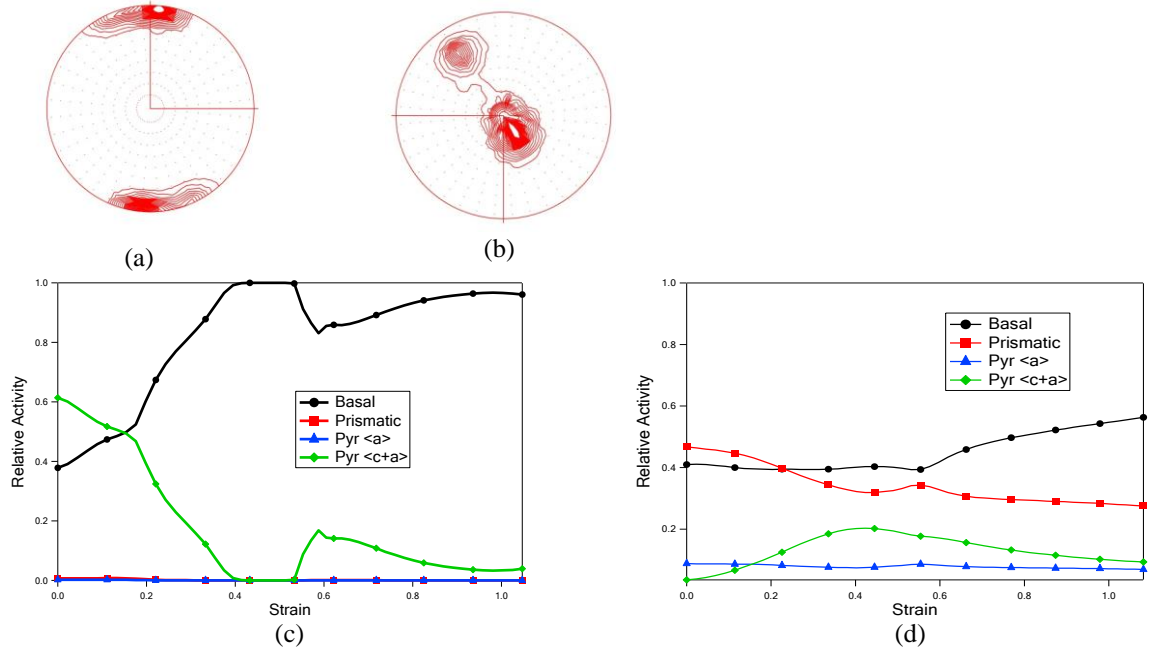
Figure 9. Predictions of the basal texture evolution and relative activities of the deformation systems for sample produced using 4A/200 °C+1A/150 °C (a, c) and 4A/200 °C+1B$_C$/150 °C (b, d).
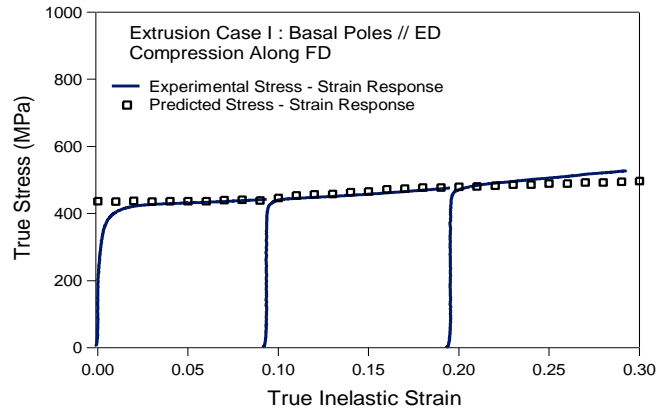
Figure 10. Comparison of experimental and predicted stress-strain response for Zr.

One of the significant benefits to the VPSC model is the ability to evaluate "a priori" potential processing routes to determine what combination of temperatures and routes will produce a sample with the desired microstructural state and mechanical properties. By using this capability, a series of hybrid routes consisting of temperature step-downs and pass combinations were evaluated to identify those that yielded alloys with ultrahigh strengths and reasonable ductility. The mechanical response for AZ31B subjected to a variety of processing routes is shown in figures 11 and 12. An explanation for the directions provided in the figures is given in the schematic of the ECAE process.
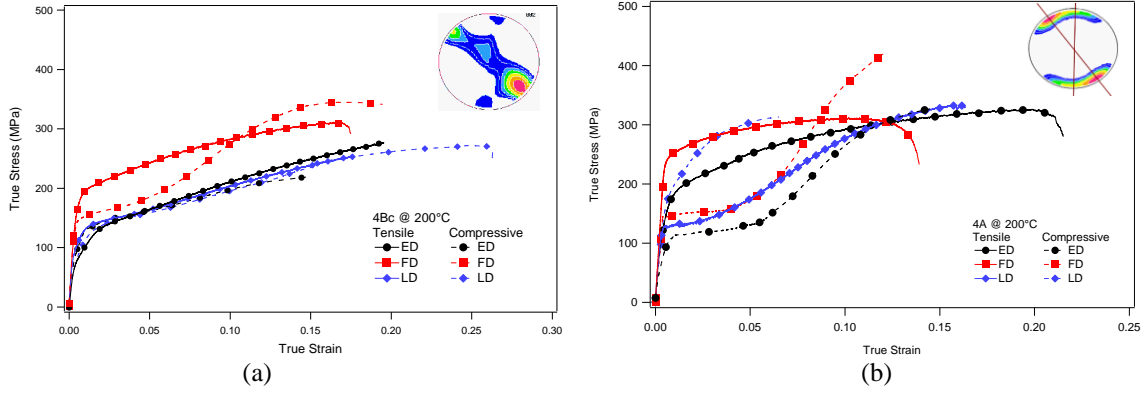
Figure 11. Reduced or enhanced anisotropy in the room temperature tension (a) and compression response of ECAE processed AZ31B Mg alloy (b), depending on the ECAE route design.
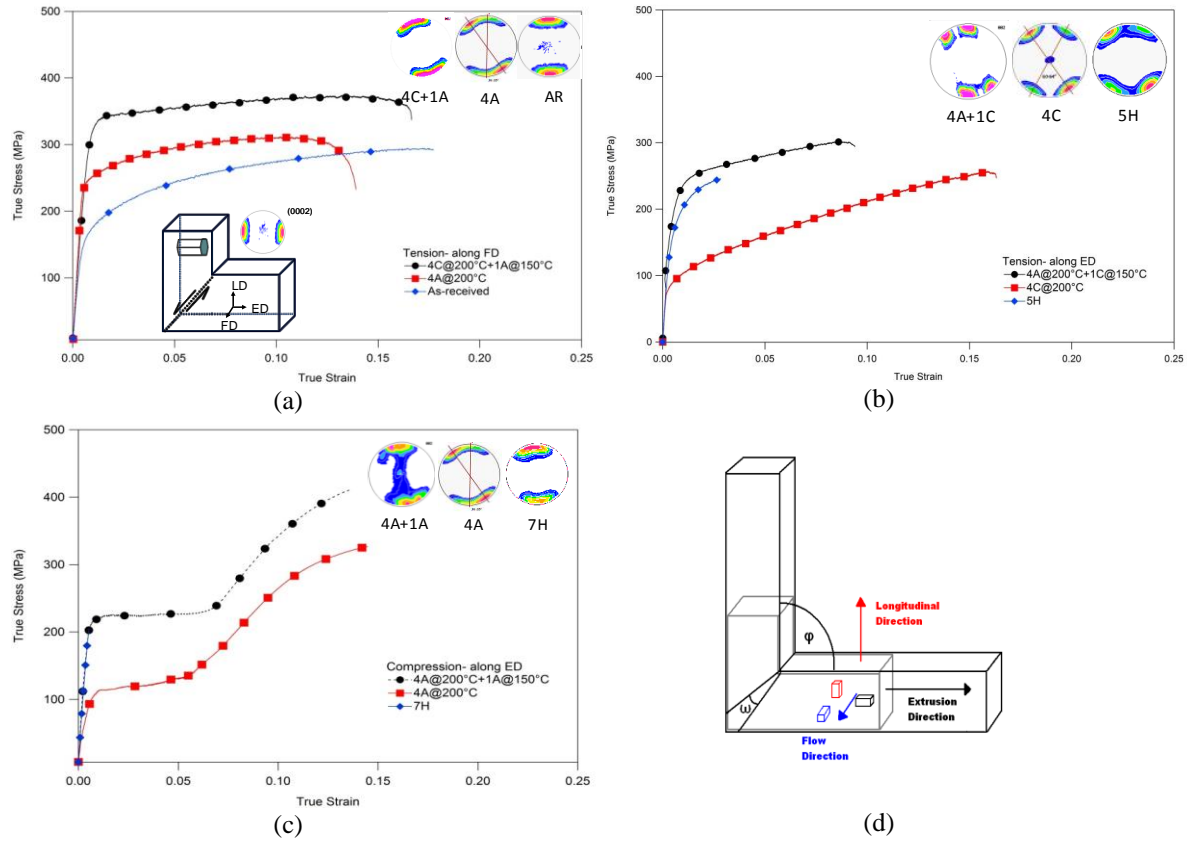
Figure 12. The effect of hybrid routes on the resulting tension and compression response of ECAE processed samples for (a) tension along the flow direction (FD), (b) tension along the ED, and (c) compression along the ED, indicating the significant enhancement in strength levels without sacrificing ductility. A schematic explaining the different directions referenced in previous figures is given in (d).

Once appropriate processing routes were established, attention shifted to determining the influence of grain size and/or slip systems on the mechanical properties of AZ31B. The use of VPSC models enabled routes to be designed that effectively isolated slip systems such that definitive observations could be made regarding the effect of grain size on their response. For example, shown in figure 13 are the stress-strain curves for the indicated deformation mechanisms. Grain size hardening of prismatic slip and tensile twinning seems to be very pronounced. However, basal slip showed a small hardening as the grain size was reduced. The data from these figures is plotted along with data collected from the literature in figure 14. Table 2 provides an explanation regarding the processing routes used for samples shown in figures 12 and 13.
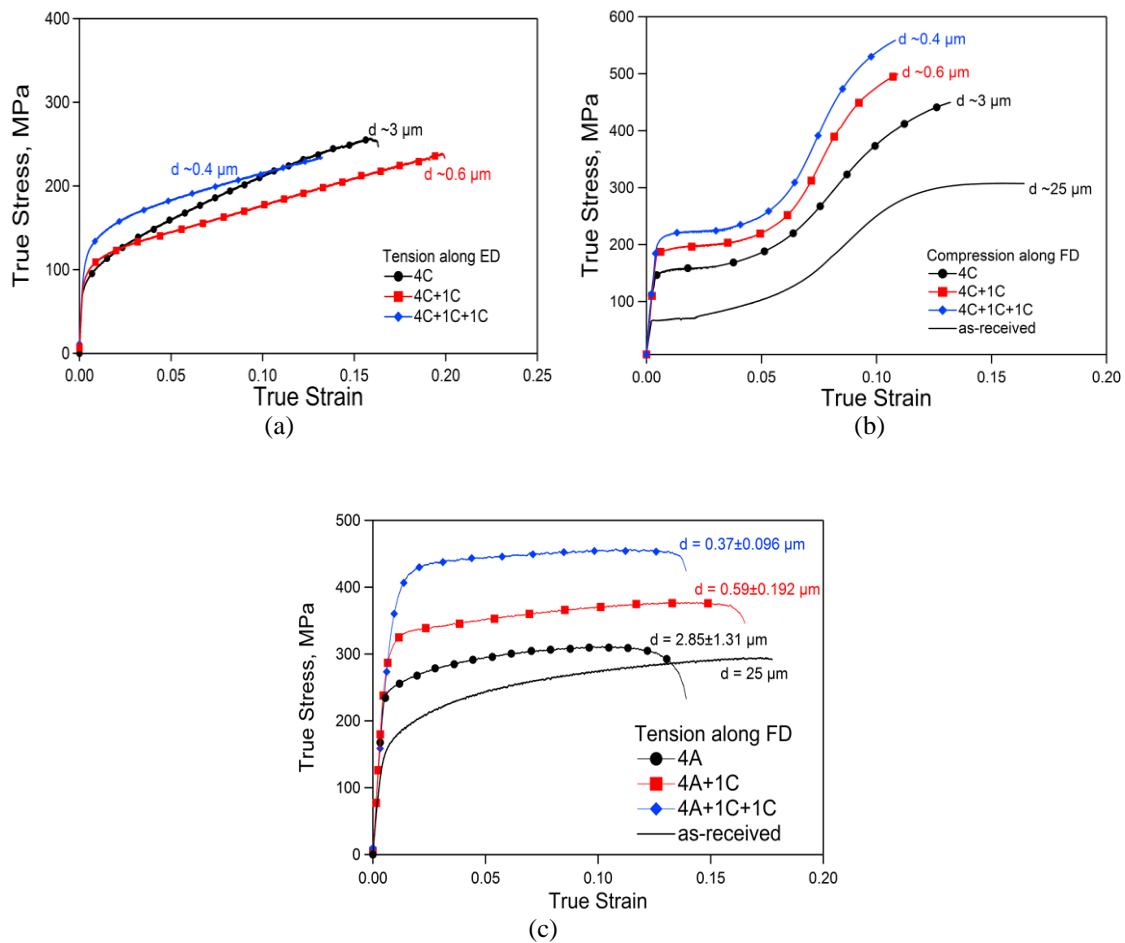
Figure 13. Effect of grain size on hardening of different deformation mechanisms: (a) basal slip, (b) tensile twinning, and (c) prismatic slip.
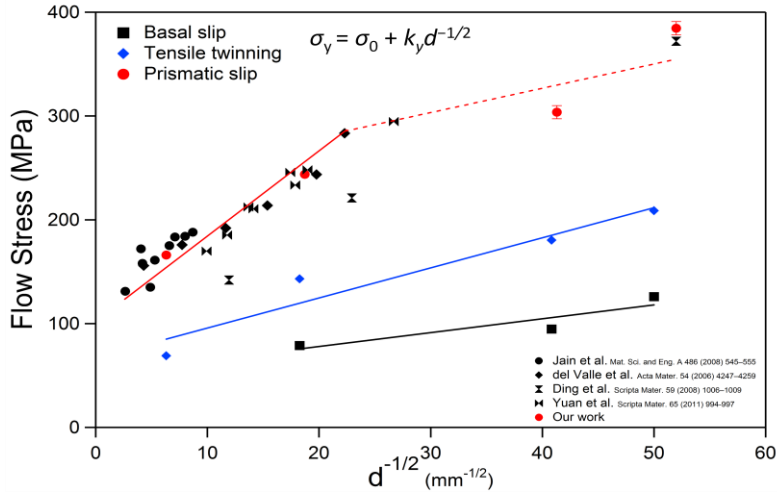
Figure 14. Flow stress as a function of grain size for AZ31B.

Table 2. Processing routes corresponding to indicated symbols in figures 12 and 13.

Symbol	Processing
4A	Four passes of route A at 200 °C; no rotation between passes
4C	Four passes of route C at 200 °C; 180° rotation between passes
4A+1C	4A plus a 180° rotation, then one additional pass at 150 °C
4B$_c$	Four passes of route B$_c$ at 200 °C; 90° rotation between passes
4C+1C	4C plus a 180° rotation, then one additional pass at 150 °C
4A+1C+1C	4A+1C plus a 180° rotation, followed by a final pass at 125 °C
4C+1C+1C	4C+1C plus a 180° rotation, followed by a final pass at 125 °C
5H	2A at 200 °C + 180° rotation + 2A at 150 °C + 180° rotation + 1A at 125 °C
7H	4A at 200 °C + 180° rotation +2A at 150 °C + 1A at 125 °C

Continued use of VPSC modeling provided insight into the importance of suppressing nonuniform deformation and twinning during ECAE processing. The photos in figure 15 are of two sets of samples processed using different routes. The samples on the right contain deep shear bands, which are undesired effects of processing. The VPSC model was used to identify the relative activity of the different deformation mechanisms during each part of the processing runs, as illustrated in figure 16. From the respective plots, it can be determined that the presence of twinning in the second sample results in discontinuous dynamic recrystallization and shear localization. This example points out a key feature of VPSC models; namely, that they allow us to a priori determine suitable processing routes for obtaining specimens with the desired microstructure.
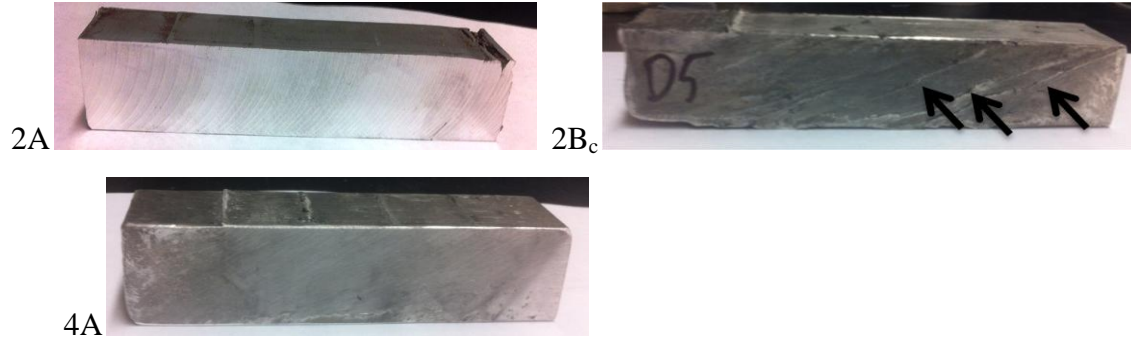
Figure 15. Photographs of AZ31B samples prepared using indicated route at 150 °C. Samples processed using A-based routes are free of the shear bands seen in the sample produced using route 2B$_c$. (Arrows indicate the shear bands in the latter sample.)
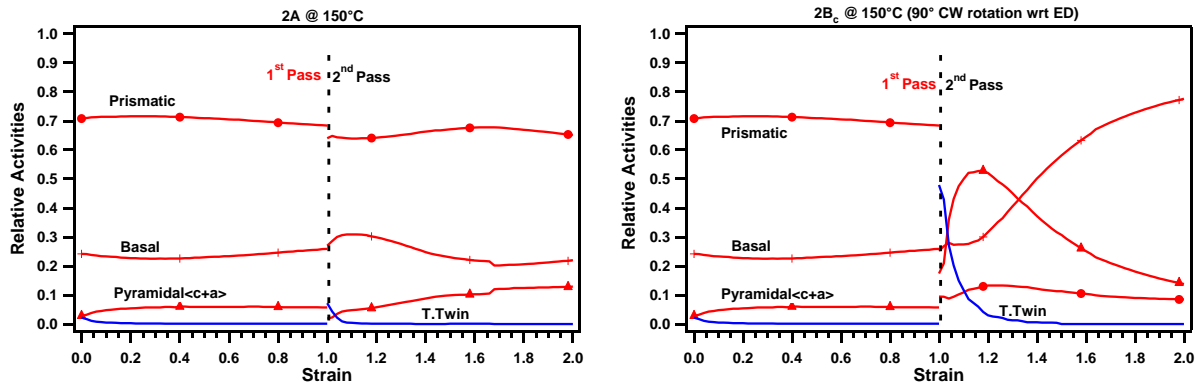
Figure 16. VPSC model results providing insight into which deformation mechanisms result in processing-related defects in AZ31B billets. In this case, the presence of tensile twinning at the initial stages of the second pass in the 2B$_c$ billet resulted in the shear bands observed in the photograph in figure 15.

To produce larger samples for use in a wider range of testing, including ballistic properties, a 6- × 6- × 1/2-in die for processing plates was made. Shown in figure 17 is an AZ31B plate sample that has been partially processed through one ECAE run. The grid lines provide an illustration of the deformation that occurs during an ECAE cycle. Experiments to date have indicated that the behavior observed in bar samples can be replicated in plate samples (see figure 18). Moreover, the plate geometry also allows for rotation about the plate normal (figure 19), thereby opening up new processing pathways.
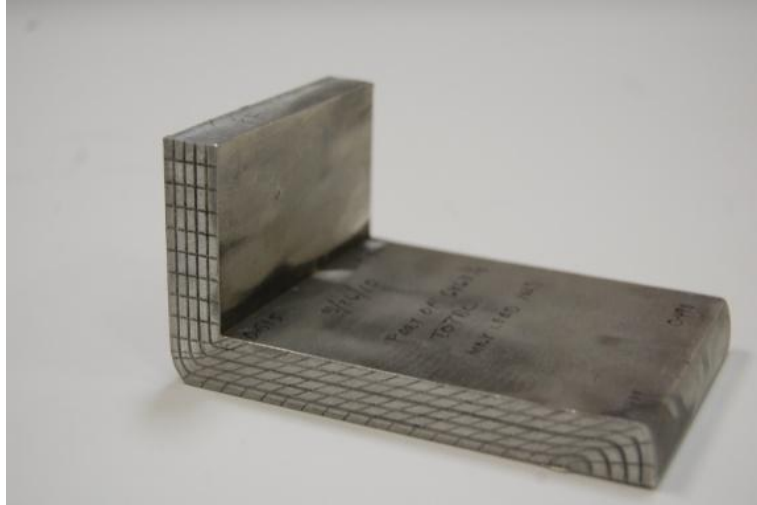
Figure 17. Photograph of 6- × 6- × 1/2-in AZ31B plate sample that has
been partially ECAE processed.
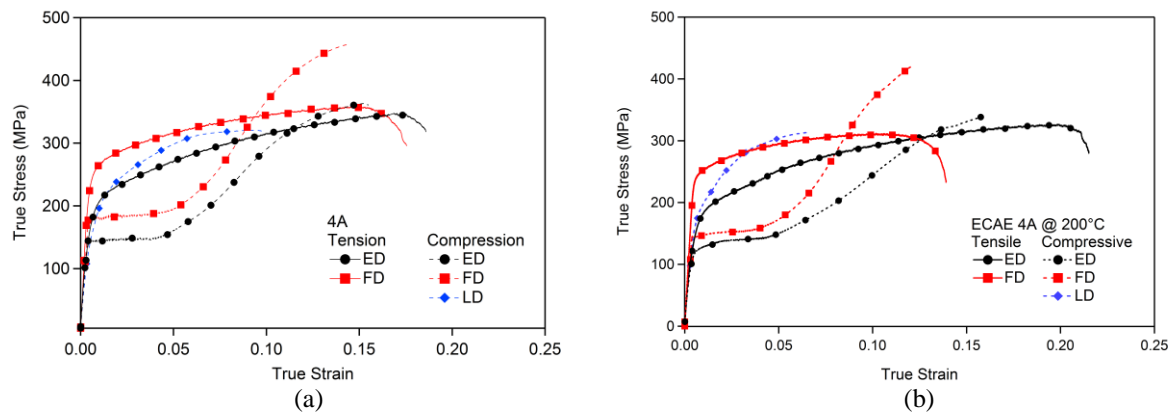
Figure 18. Comparison of (a) stress-strain curves for plate and (b) bar samples subjected to 4A/200
°C processing cycle.
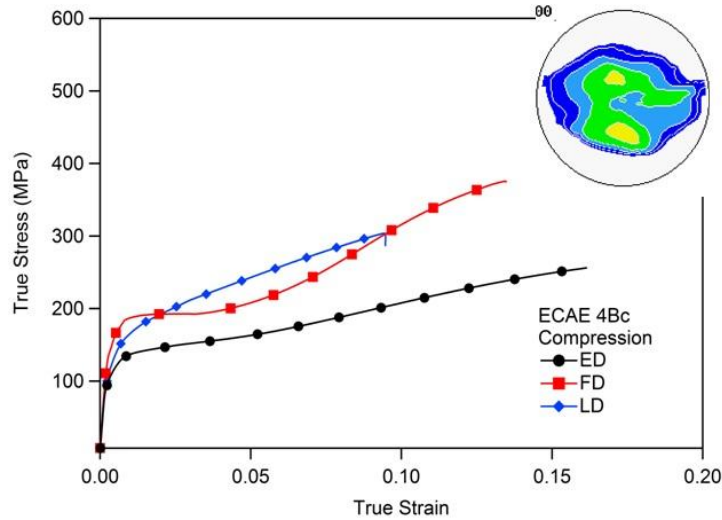
Figure 19. Stress-strain curves and texture map for plate sample rotated about the plate normal (4B$_c$/200 °C).

Since its inception, a primary objective of this effort was to determine if the microstructural refinement (grain size and random texture) and subsequent property improvements gained through ECAE processing would result in improved ballistic performance of Mg alloys. Following the demonstrated ability to achieve similar property improvements in plate samples that were originally accomplished in bars, this goal is now becoming a reality.

Indeed, an initial evaluation has been performed on a limited number of 6- × 6- × 1/2-in plate samples processed at Texas A&M University. Three sets of samples were provided: as received, texture A, and texture C. Texture A samples were produced using the recipe 2A + 1C (all at 250 °C) + 1A at 200 °C + 2A at 150 °C. Texture C samples were produced using the recipe 2A at 250 °C + 2C at 200 °C + 2C at 150 °C. Because of their thickness, the plates were tested only against 17-gr FSP threats. Test results, shown in table 3, indicate that the there was approximately a 3.5% and 5.2% improvement, respectively, in the ballistic limit for the texture A and texture C plates. Representative pictures of the front and back plate surfaces after ballistic testing are shown in figure 20. The top row of photos is the front of the plate and the bottom row is the back of the plate. Surface cracks can easily be seen in some of the ECAE-processed plates (c, d).

These results are encouraging, particularly given the presence of surface cracks in the ECAE processed plates that are thought to have an adverse influence on performance. Current plate processing efforts are focused on eliminating the cracks through the use of an applied back pressure, thereby resulting in improved properties and potentially higher ballistic performance. Ballistic testing was performed by Tyrone Jones, Armor Mechanisms Branch, Protection Division, ARL Weapons and Materials Research Directorate.

20

Table 3. Ballistic test results for ECAE-processed AZ31B plates.

Sample	Thickness (in)	Velocity (ft/s)
AR - 1	0.483	2046
Texture A	0.482	2117
AR – 2	0.462	1967
Texture C	0.462	2070
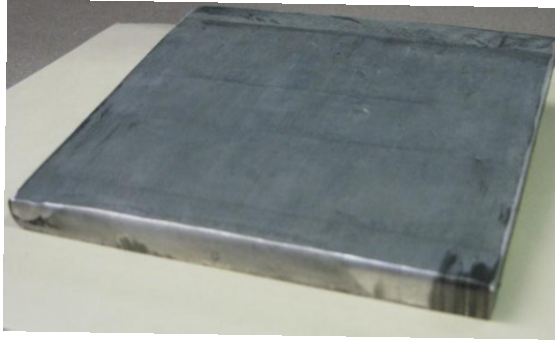
(a)
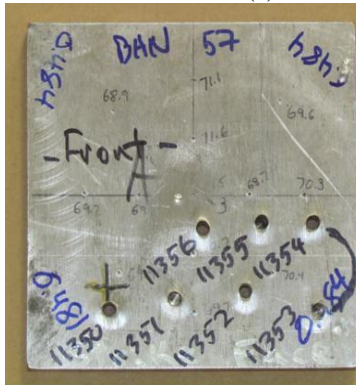
(b)

(c)

(d)

Figure 20. Photographs of (a) ECAE-processed 6- × 6- × 1/2-in AZ31B plate. Photos of the ballistic tested samples are given in (b) as received, (c) texture A, and (d) texture C conditions. The top row of photos is the front of the plate and the bottom row is the back of the plate.

5. Development of ARL In-House ECAE Capability

Based on the success of early studies conducted with external collaborators, initial funding was provided in 2007 to establish an in-house ECAE processing facility. As stated in the funding request, the creation of such a facility "would result in a state-of-the-art structural materials nanofabrication facility" and enable the "linking of the unique material properties obtained in nanocrystalline materials with specific Army needs" (*11*). In addition, establishing such a facility would ensure that developmental work could continue in areas that would be too sensitive to conduct outside ARL facilities.

With the funding provided, a hydraulic press system with a maximum load of 760,000 lb and press speed of 1 in/s was designed, constructed, and eventually installed by Shear Form Inc. in Lab 1286 of ARL's Rodman Materials Lab (see figure 21). The press frame has a movable cross-head, which when combined with the 21-in stroke of the piston allows for the processing of a broad array of sample sizes and geometries. Press operations can be controlled either by using a manual joystick or through computer software. Safety shields, switches, and interlocks are designed to protect the operator from harm in the case of tool, billet, or other system component failure.

In addition, Shear Form Inc. was also contracted to provide custom-made tooling dies for the ECAE press (figure 21). Tooling dies with the inlet-outlet channel size of 3/4- × 3/4- × 9-in bar, 6- × 6- × 1/2-in plate, and 12- × 12- × 1-in plate tool have been provided. The tooling can be heated to approximately 300 °C for the extrudate to have the necessary ductility. Finally, supporting equipment such as a high-temperature box furnace (for preheating samples prior to extrusion) as well as machining tools (mini-mill and lathe) are all installed in close proximity to the press to ensure rapid operations with minimal down-time between processing runs. Since its installation, the ECAE press has been used to process a variety of material systems, including plastics, powders, and several alloys.

Figure 21. Photographs of the ECAE press facility located at ARL, Aberdeen Proving Ground, MD. Right photo shows the tooling die for 0.75- × 0.75- × 8-in billets and the control consoles.

6.   Applied Research Relating to Magnesium Program

Through the use of ECAE processing, ARL has made significant advances in developing the capability to produce ultrahigh-strength Mg alloys. Despite this proven capability of ECAE, the method is currently limited to fairly small sample sizes. To obtain larger UFG Mg alloy plates for testing and evaluation, efforts were also undertaken using both friction stir processing (FSP) and supersonic particle deposition (i.e., cold spray deposition). Given the reality of Mg and its susceptibility to corrosion, appreciable effort was also spent in identifying potential methods for improving corrosion performance, as well as evaluating new alloys as they became available. The potential of UFG Mg alloys to improve ballistic protection, while lowering overall system weight, was evaluated in both helmet and body armor packages.

6.1   Friction Stir Processing

FSP is a solid-state process that has shown much promise for achieving significant grain refinement in Mg alloys. During FSP, friction between the moving tool and the work piece generate large amounts of heat that, in combination with the plastic deformation occurring around the tool, results in a dynamically recrystallized fine-grain structure (*12*). Not surprisingly, the grain structure of the processed piece depends strongly on processing parameters, tool geometry, and cooling rate. To fully explore the potential of FSP for producing nanograined Mg alloys, a systematic study was performed to correlate processing parameters to the final microstructure of AZ31B alloy plates.

For this study, two different tool designs were used to evaluate their influence on grain refinement (see figure 22). The first tool had a single truncated cone-type pin while the second had three blades. Both tools were designed to achieve as high a degree of grain refinement as possible in a processing zone as thick as 2.3 mm. As initial studies had indicated that appreciable grain growth could occur in the processed zone due to the increased temperature, a copper anvil that could be cooled using liquid nitrogen was also designed and used to remove heat from the plate during processing (figure 23). In addition, the top surface of the plate was cooled by flowing liquid nitrogen through two copper tubes lying parallel to the processing area. Cooling tests prior to processing trials indicated that the plate temperature could be lowered to –180 °C through the use of active cooling.

Truncated cone pin   Three-bladed cone pin
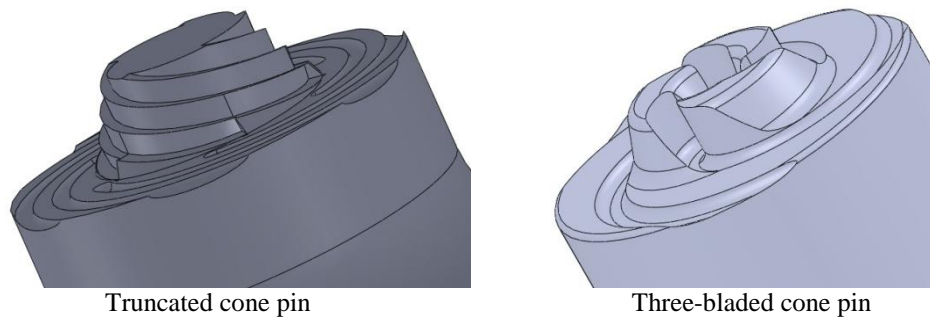
Figure 22. Illustrations of the two types of tools used in the friction stir processing trials.
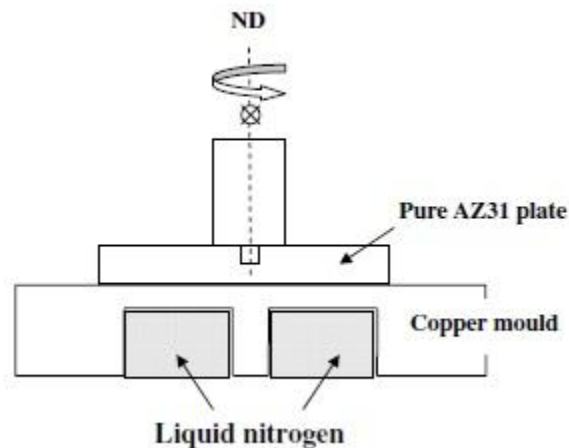
Figure 23. Schematic of the active liquid nitrogen
cooling plate used in an attempt to
minimize grain growth that occurs during
processing of AZ31B plate material.

Table 4 provides the tool type, spindle speed, and travel speed combinations for the different processing runs. The effect of active cooling on final grain size was determined by running similar conditions in both ambient and liquid-nitrogen-cooled conditions. Optical micrographs showing the difference in weld zone for samples processed using the truncated cone pin at a travel speed of 356 mm/min are shown in figure 24. After each processing run, grain size analysis was conducted using both optical and orientation imaging microscopy (OIM) on a TexSEM Laboratories Incorporated TSL OIM EBSD system. Results for optical microscopy are shown in figure 25, while those for OIM are given in table 4. On a comparative basis, the truncated cone pin tool appears to achieve a higher degree of grain refinement. Values seen in these figures are significantly higher than those given in table 4, obtained using orientation imaging microscopy. Values in table 4 are deemed more accurate due to the increased resolution and accuracy of OIM relative to optical microscopy. Comparison of the results indicated a significant disparity in grain size measurements, with values measured by OIM being approximately one-third those measured by optical microscopy. This disparity was attributed to the inherent resolution and increased accuracy of OIM relative to optical microscopy.

Table 4. Combination of processing parameters used in the study. Grain size and temperature data are for actively cooled plates only. Grain size measurements were performed using orientation imaging microscopy.

Tool Type	Spindle Speed (rpm)	Travel Speed (mm/min)	Grain Size (nm)	Measured Root Temperature (°C)
Truncated cone pin	1200	762	2100	—
	1200	508	2400	200
	1200	356	2900	225
Three-bladed cone pin	1000	762	3300	250
	1000	635	3200	270
	1000	508	3200	300
	1000	381	3200	—

Ambient   Chilled
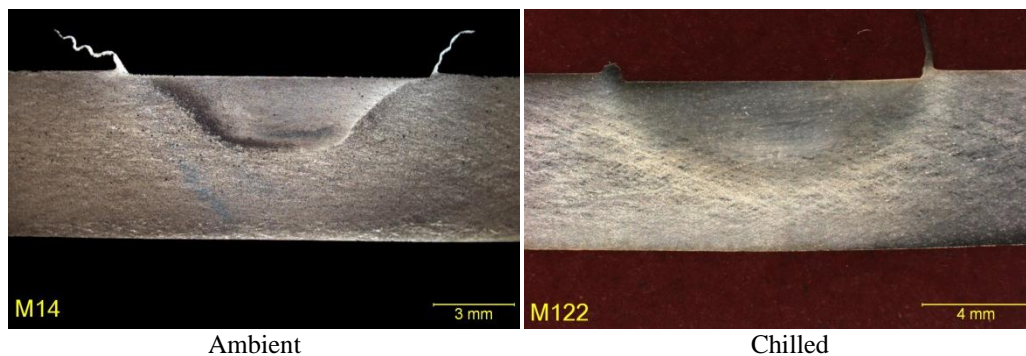
Figure 24. Optical micrographs for samples processed using the truncated cone pin, 356-mm/min travel speed.
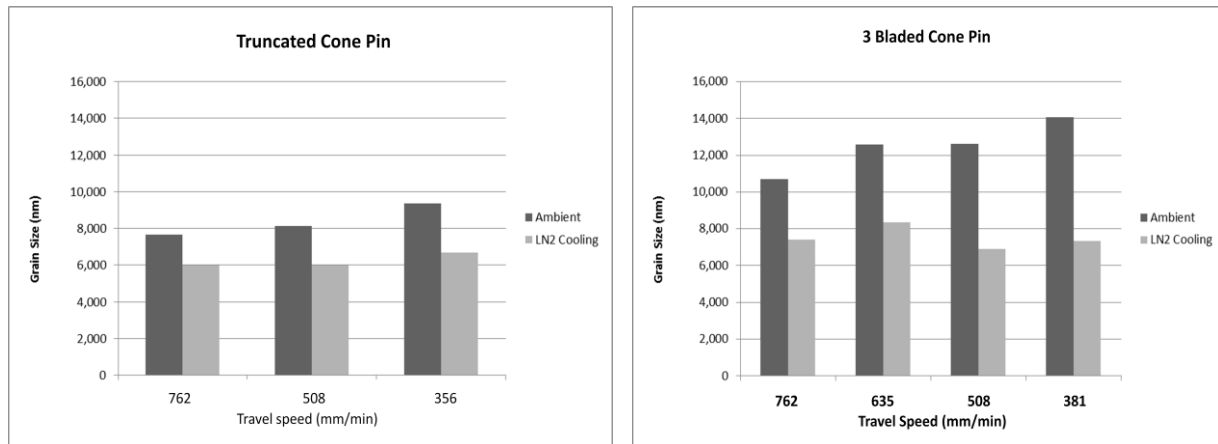
Figure 25. Grain size measurements obtained using optical microscopy.

The data shown in figure 25 indicate that finer grain sizes are obtained for the actively cooled samples regardless of travel speed. Temperature measurements collected using thermocouples directly beneath the work affected zone in the plates processed using the truncated cone pin confirmed this observation (table 4). However, grain size is essentially constant in the plates processed using the three-bladed cone pin, suggesting that there is complex effect on grain size due to the combination of tool geometry and strain rate. Finally, the measured grain sizes were well above the target goal of 500 nm. Since the use of liquid nitrogen cooling only resulted in grain sizes on the order of 2000 nm, other methods for lowering the heat input/temperature of the work zone need to be considered. Although calculations indicate that lower temperatures could be achieved by using a tool one-half to two-thirds smaller than the truncated cone pin tool, such a design would, by necessity, result in a negative impact on the volume of material processed per unit time. Efforts to identify viable solutions for reducing the work zone temperature remain the focus of ongoing work.

6.2   Cold Spray

Mg alloys are of great interest in a variety of industrial and military applications due to their low densities and high strength-to-weight ratios. The current program was designed to investigate novel processing techniques for producing large-scale bulk samples of Mg for vehicle applications, with a specific focus on ballistic protection.

One of these techniques was cold spray, a thermal spray-type technology that consolidates powdered metals through heat and kinetic energy. Depositing metal powders onto substrates to form bulk materials using cold spray technology has several advantages over other methodologies. The melting temperature of the material is not reached during cold spray, which essentially cold-works the solid state particles, increasing the hardness and ultimate strength.

Furthermore, the low temperature of the spray process allows for the deposition of thermally sensitive materials such as Mg. The typical cold spray deposition process involves accelerating metal particles into the surface layer of a substrate at high speeds. Figure 26 shows a simplified diagram of a typical cold spray setup. As these particles impact the substrate surface, both the particle and the surface are deformed plastically, thereby allowing the particles to adhere mechanically to the surface and each other. This deformation leads to highly dense deposits with strengths equal to or greater than wrought structures of the same material. The final thickness of the deposition layer is determined by the length of the deposition process. The ability to scan the surface determines the final area covered by the deposit.
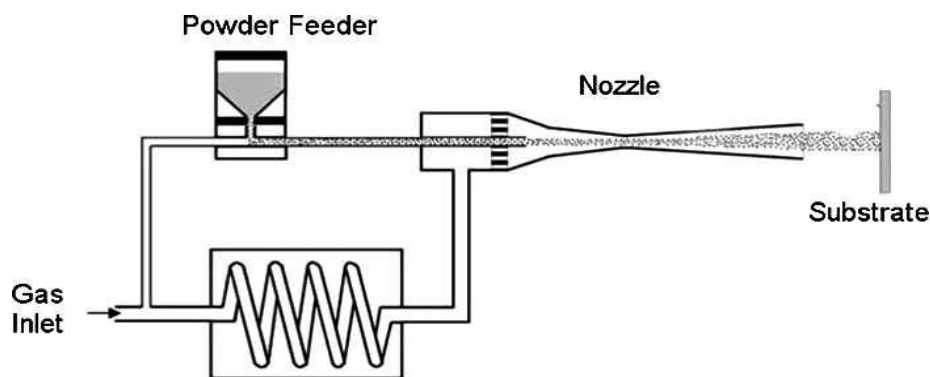
Figure 26. Cold spray process.

Consolidation of Mg by cold spray is a relatively new effort and is based upon ARL's much more extensive work with Al due to the similarity of these two light metals. However, Mg and its alloys present a number of unique challenges compared with Al that had to be addressed during the program.

First and foremost, the supply of high-quality Mg alloy powders is extremely limited. Only one vendor has legacy alloys available in powder form, and these production capabilities are so new that meeting the requirements for optimum cold spray feedstock was challenging. For example, the majority of the powders used in these trials were milled, which imparts a number of detrimental characteristics to the powder prior to spraying. The powders are exposed to the milling environment, which can cause contamination and excess oxidation. Also, the milling process itself imparts cold-work to the powder particles, which reduces the ease with which they plastically deform upon impact in the cold spray process. Finally, the milling process leads to widely distributed powder sizes with irregular shapes, which reduces cold spray efficiency.

Mg and its alloys are also less ideal cold spray candidates than Al because of the crystal structure of Mg. Al, as a face-centered cubic (fcc) metal, is often grouped with copper as a model cold spray system due to the large number of slip planes present in the fcc lattice. This facilitates plastic deformation on impact, which is crucial to successful deposition. The extreme deformations allow for the exposure of fresh metal surfaces, which help form chemical and

27

metallurgical bonds at the particle-substrate and particle-particle interfaces. This increases both the adhesive strength of the coating to the substrate and the cohesive strength of the particles to each other for higher coating integrity. In contrast, hexagonal close-packed (hcp) metals like Mg and titanium have fewer slip planes, increasing the energy necessary to produce adequate impact deformation for high-quality deposits. When particle deformation does not occur, the undeformed particles can act as a "shield" for subsequent cold spray passes, potentially resulting in pores in the final coating. However, due to the thermally sensitive nature of Mg, this energy increase must come from higher cold spray pressures as opposed to temperatures. It is possible that current cold spray technology is unable to produce sufficient pressures to adequately deform large Mg particles at appropriate operating temperatures.

Mg's extreme temperature sensitivity presents particular challenges for powder handling, storage, and deposition. There is evidence to suggest that there are competing factors contributing to the deposition efficiency (or lack thereof) of Mg powders. It is well established that softening a given powder by heating it during acceleration in the cold spray system is crucial to making the particles more malleable, yielding a denser, stronger coating. However, even the mildest of temperature settings for deposition led to visible oxidation and discoloration of the deposit once it was outside the direct line of the spray nozzle and the flow of inert carrier gas. This oxidation is very likely to be a contributor to both the high strength and low ductility of the bulk Mg samples. Moreover, the hard, brittle nature of the surface oxide makes for a poor cold spray substrate, as the opportunities for interlocking metallurgical bonding would be diminished by the lack of surface plasticity. These factors led to a trend of low deposition efficiencies of 30%–40% and generally low-quality deposits with high porosity and residual undeformed particles. Improvements in powder handling, such as degassing, as well as surface protection techniques employed during deposition, may improve both the quality and efficiency of Mg consolidation.

6.2.1 Cold Spray of AZ31B

AZ31B produced the highest quality coatings in initial trials, leading to a temperature optimization study. The minimal porosity in the initial coatings was significantly reduced by increasing the operating temperature, leading to a fully dense coating. Optimal deposits were achieved at 350 °C, as measured by deposition efficiency, areal percentage of undeformed particles, and porosity (figure 27).
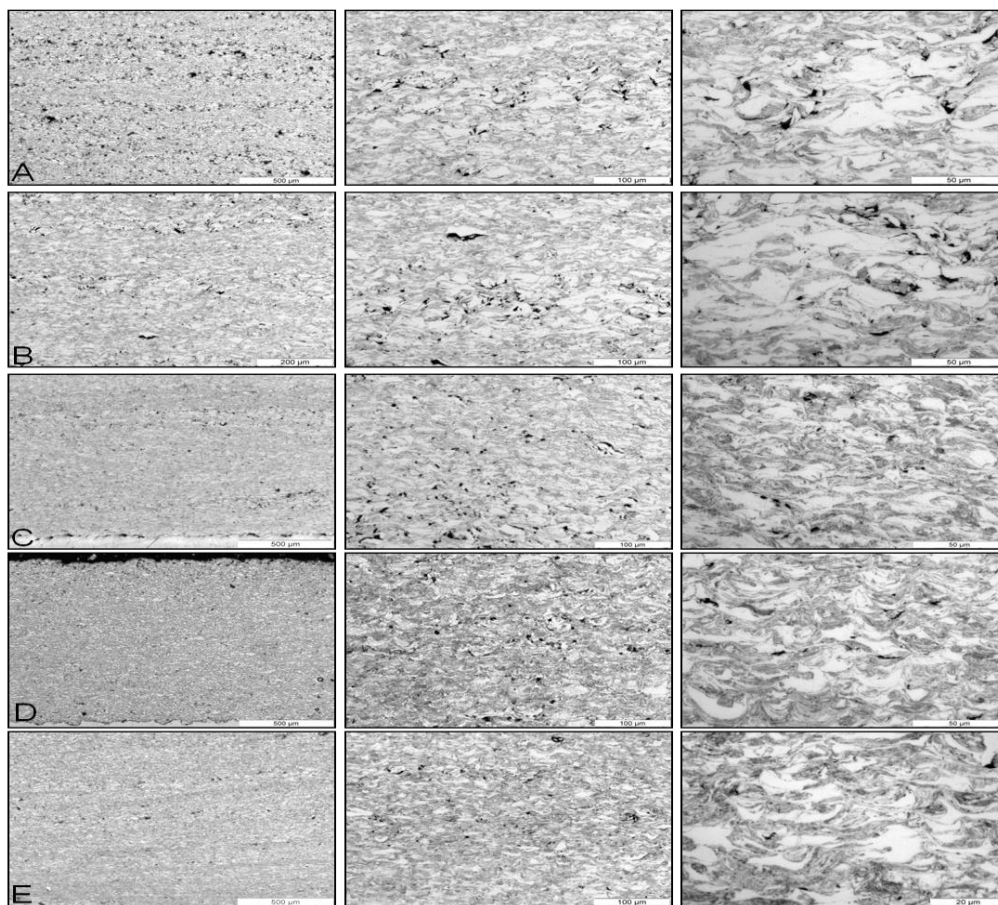
Figure 27. Micrographs taken for AZ31B deposited using cold spray at driving gas
temperature of (A) 200 °C, (B) 250 °C, (C) 300 °C, (D) 350 °C, and (E) 400 °C.

Despite being the most thoroughly investigated alloy in the preliminary study, lack of available powder supply prevented further characterization of mechanical samples. Results of the AZ31B optimization study were used in an attempt to produce fully dense deposits from other alloy powders, namely WE43 and Elektron 21. Representative micrographs for deposited material are shown in figure 28.

| (a) | (b) | (c) |
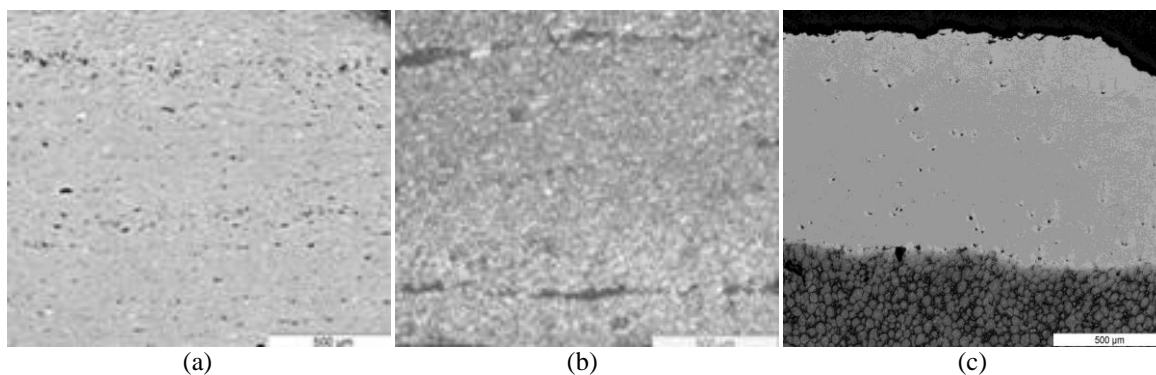
Figure 28. Representative micrographs for cold spray deposited (a) WE43, (b) Elektron 21, and
(c) atomized WE43.

6.2.2 Ground WE43

Ground WE43 was received as a coarsely ground powder with a wide size distribution and irregularly shaped particles. This led to difficulties in consolidation because any given set of spray parameters would be suboptimal for a large portion of the feedstock at any given time. Furthermore, despite the mean size of the powder being less than 30 μ, the distribution was skewed with a number of larger-sized particles. Critical velocity was unattainable for many of the larger particles, leading to low densities and a number of undeformed particles embedded in the coating. This reduced the coating density and cohesion, leading to porous, low-strength deposits. Slight improvements were made by sieving the powder to remove large particles, yielding a smaller mean diameter (20 μ) and a narrower distribution, but coating porosity remained a problem at over 5%. Given the poor deposition quality, it was decided not to pursue the production of larger-scale plates suitable for mechanical testing.

6.2.3 Elektron 21

Elektron 21 alloy powder suffered from many of the same problems as ground WE43 powder. The presence of large particles and the associated skewed distribution led to difficulty in optimizing spray parameters. Even after sieving, the powder consolidated with more than 11% porosity, which was deemed an insufficient density to pursue larger-scale consolidation.

6.2.4 Atomized WE43

Development of increased atomized Mg capability through a cooperative effort between Hart Metals, Inc., and the U.S. Army led to the procurement of atomized WE43 powder. The size and shape of the atomized powder were much more compatible with the cold spray process. Spherical powders deform more uniformly on impact compared with powders with higher aspect ratios. Furthermore, the atomized powder order was delivered prescreened to -325 mesh (less than 44 μ), reducing the detrimental effects of large particles on deposition. Based on the optimal parameters for AZ91B, WE43 was sprayed to full density in early trials. The high density, lack of undeformed particles, and high (for Mg) deposition efficiency of 40% resulted in cold spray plate material suitable for mechanical testing.

Shown in figure 29 are the tensile stress-strain curves obtained from samples taken from a spray deposited plate, with the tabulated results given in table 5. Because the as-sprayed material exhibited an extremely low ductility, subsequent samples were subjected to an annealing treatment prior to tensile testing. However, as seen in the experimental data, the annealing treatments failed to have any significant effect on the properties of the deposited material. As a result, no further effort is anticipated in this area.
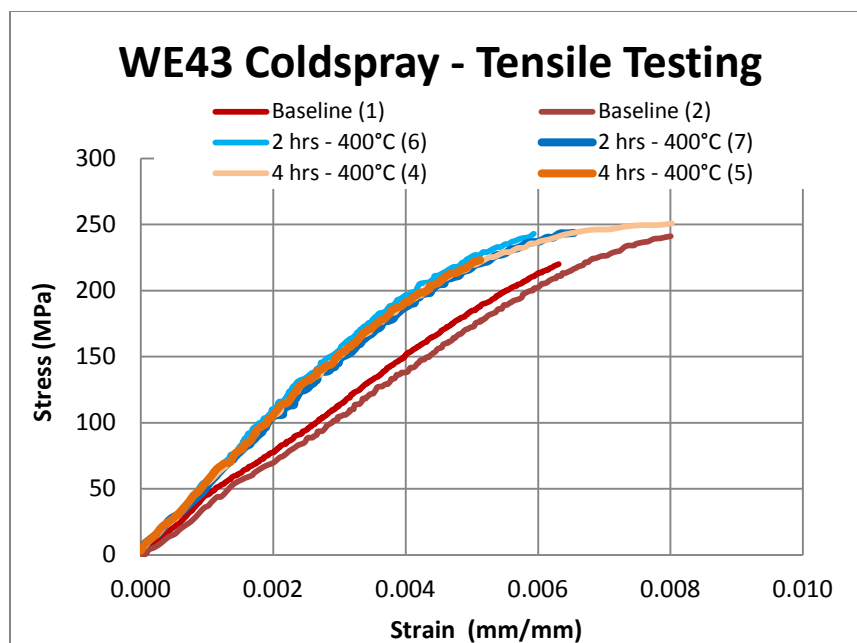
Figure 29. Tensile stress-strain curves for samples obtained from cold spray–
deposited WE43 plates.

Table 5. Tensile properties obtained from as-sprayed and annealed WE43 plate material
produced by cold spray deposition.

Properties	Baseline	Anneal 400 °C/2 (h)	Anneal 400 °C/4 (h)
Ultimate tensile strength (MPa)	232.0 ± 17.0	243.5 ± 0.71	237.0 ± 19.8
Elongation (%)	0.72 ± 0.13	0.62 ± 0.04	0.66 ± 0.21
Modulus (GPa)	38.1 ± 1.27	51.4 ± 3.96	50.8 ± 0.42

6.3   Corrosion Studies

The corrosion rate of Mg and its alloy is the highest of all metals being investigated for use as armor by the Army and can be attributed to two primary factors. First, due to an inherently low corrosion potential in corrosive environments, nearly any alloying addition or contaminant present in the alloy will serve as the site of local cathodic reactions, mainly hydrogen evolution. Second, although Mg, like most metals, will form a surface oxide, the oxide layer does not form a stable protective film like other metals (such as Al oxide). Rather, the film will break down, thereby continually exposing "fresh" Mg metal to the corrosive environment. Mitigating metallic corrosion may be accomplished by compositional changes to the alloy chemistry, as well as with active or passive coatings.

A fundamental understanding of the galvanic corrosion mechanisms occurring in new and commercially available alloys is crucial to developing solutions to the Mg corrosion problem. Using macroscale cyclic corrosion and electrochemical interrogation, we have been able to

understand the differences in the corrosion rate and cathodic behavior of Mg, AZ31B, E21, E675, AMX602, WE43, AZ91, and ZAXE1711. Figure 30 shows the macroscale corrosion of each of these alloys after being exposed to a corrosive environment (*13*). Similar results were observed using GM9540P cyclic corrosion tests. Electrochemically, there are significant differences between these alloys (figure 31). One particularly interesting feature of these curves is the variation of open circuit potential that results from different alloy chemistries. (A detailed description of the results in figures 30 and 31 is being prepared as an ARL technical report to be submitted during the first quarter of fiscal year 2014.) Building upon this understanding of the effects of chemistry on galvanic and general corrosion is ongoing at smaller length scales.

CP Mg (72 Hours) AZ31B AZ91C

EV31A AMX602 WE43-T5

ZE41A ZAXE1711
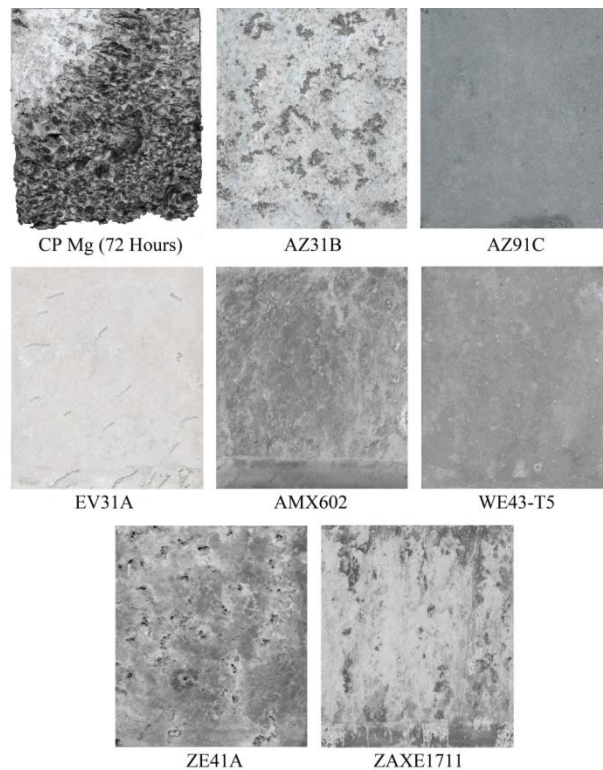
Figure 30. Images of corroded Mg alloys after 168 h in
neutral salt fog (*13*). Due to the severity of
corrosion, the commercially pure Mg sample,
top left, is photographed after only
72 h of exposure.
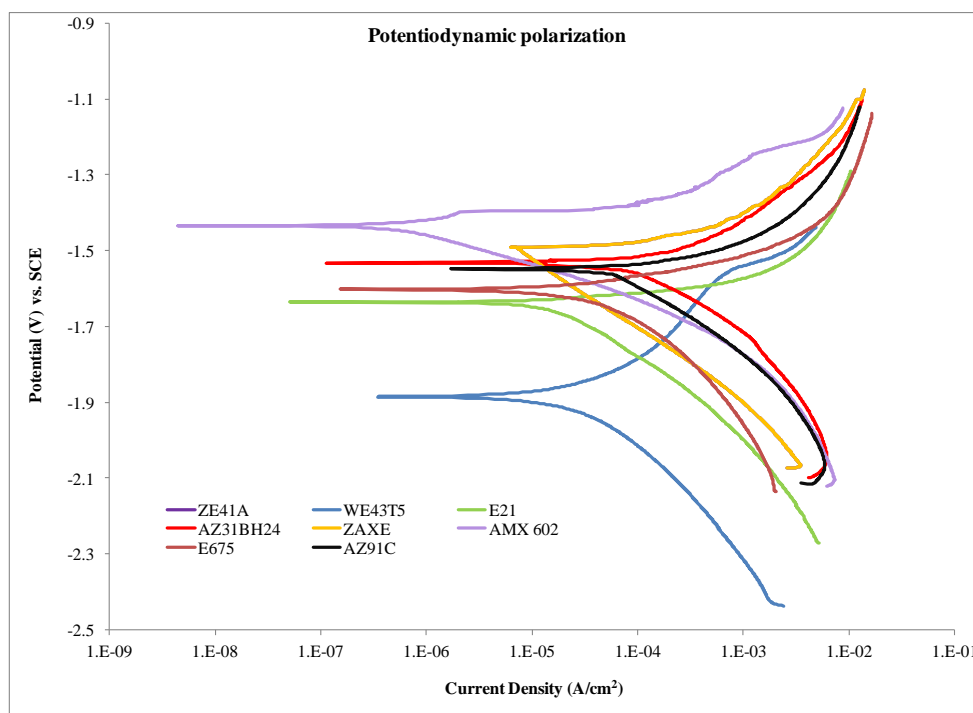
Figure 31. Representative potentiodynamic polarization curves of several Mg alloys.

Mitigation of Mg corrosion using a coatings-based approach is being explored both within ARL and through collaborative efforts with several universities (e.g., University of Virginia and Ohio State University). Recent research has focused on improving the properties of Tagnite coatings, which are the most commonly used protective coatings for Mg. Preliminary results of this work indicate that Tagnite does indeed impart corrosion protection to Mg alloys; however, the anodically grown, proprietary oxide is porous and full of defects (figure 32). We have developed a method of sealing the cracks and pores of Tagnited surfaces. This sealing process significantly reduces diffusion through the anodized layer and should allow for good adhesion to the now-sealed Tagnite. (Invention disclosure documentation is being filed with the ARL patent office regarding this process, and the details will be released to the greater community as soon as possible.) Figure 33 is a schematic representation of electrochemical impedance spectra collected from current experimental efforts that clearly demonstrate the improvement in performance obtained from the sealed coatings.
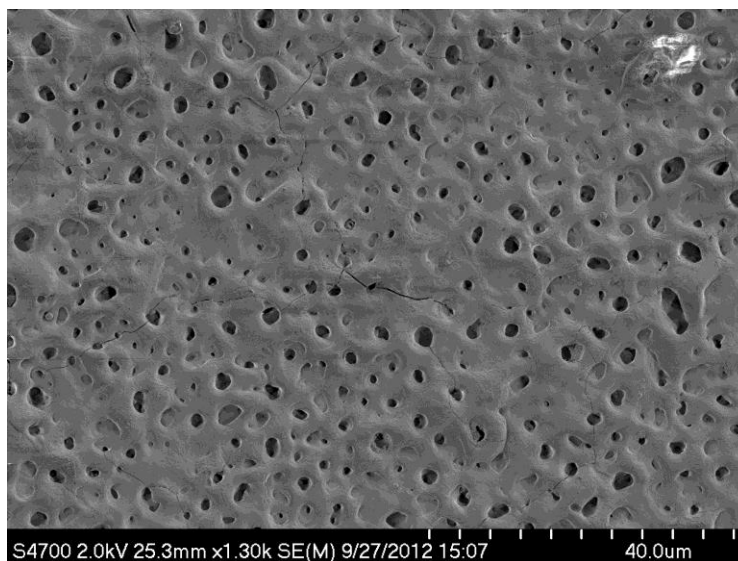
Figure 32. Scanning electron micrograph of Tagnite-coated WE43.
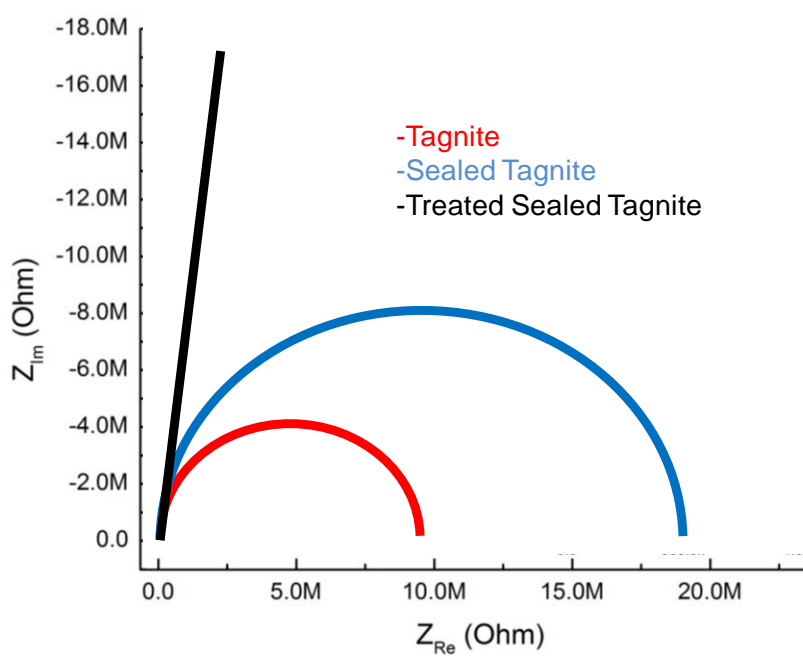
Figure 33. Idealized electrochemical impedance spectra of
Tagnite-coated Mg also coated with two different
versions of a proprietary sealer being developed at
ARL.

Although these results indicate that the already outstanding performance of Tagnite coatings can be improved, issues still exist with this coating system. Because the process results in a hard, tightly packed magnesium oxide coating with a surface deposit of fused silicates, it is often difficult to detect cracks in the alloy beneath the coating. In addition, as it is an anodized coating, repair of a damaged coating can be quite difficult. Furthermore, this coating system cannot be used to protect mixed metal assemblies from corrosion.

Thus, in an effort to develop more-user-friendly coatings, a limited effort has been conducted to evaluate the efficacy of a polymer-derived ceramic (PDC) corrosion coating. As PDCs are typically liquid or easily dissolved in a solvent at room temperature, they represent a low-cost material capable of coating complex shapes. After the polymeric film is applied, a conversion treatment (either at moderate temperature or in ultraviolet light) transforms the film into a highly inert ceramic coating. The potential of a PDC as a corrosion coating for Mg was demonstrated by Motz et al. (*14*), who applied a thin (less than 5 µm) silicon carbon nitride (SiCN) coating to Mg sheet that was then exposed to a 5-mass% sodium chloride solution. In contrast to an uncoated Mg sheet that showed extensive corrosion after just 1 h, the coated sheet showed no indication of corrosion after 5 h.

Working in collaboration with scientists from the University of Colorado, a polysilazane coating was applied to the surface of the AZ31B samples using a laboratory bench-top spin coater. The resulting SiCN coating was approximately 0.25-µm thick and contained pinholes and entrapped dust due to deposition in a nonclean room level environment. The transparent nature of the coating is shown in figure 34, which compares an uncoated and coated sample.

AZ31B uncoated   Polysilazane coated
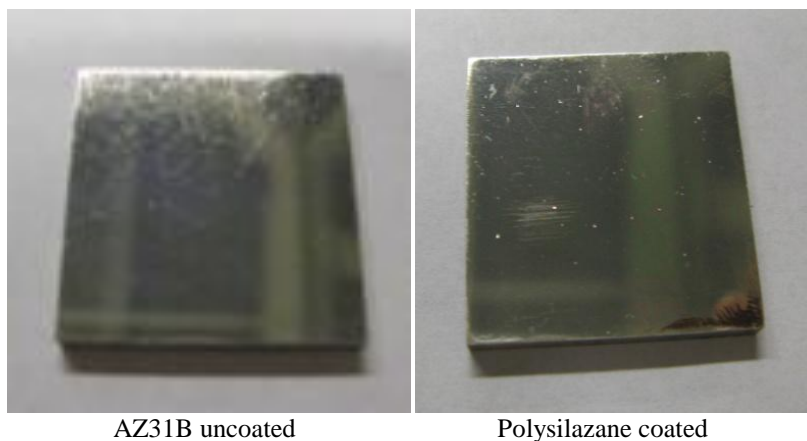
Figure 34. Optical micrographs of uncoated (left) and polysilazane coated
(right) AZ31B sample.

Despite the thinness and relatively poor quality, the polysilazane coating provided a measure of protection to the Mg alloy, as shown in figure 35, which details the results from potentiodynamic polarization and electrochemical impedance (EIS) measurements. The polarization curves clearly demonstrate the superior corrosion performance of the sample coated with Tagnite. The polysilazane-coated sample shows a slight reduction in the current measured at the open circuit potential, which indicates a slight improvement in corrosion performance. A similar pattern of performance can also be seen in the EIS results, in which a larger "hump" in the curve indicates a better corrosion resistance. The improvement in corrosion performance for the polysilazane coating is more apparent in this figure.
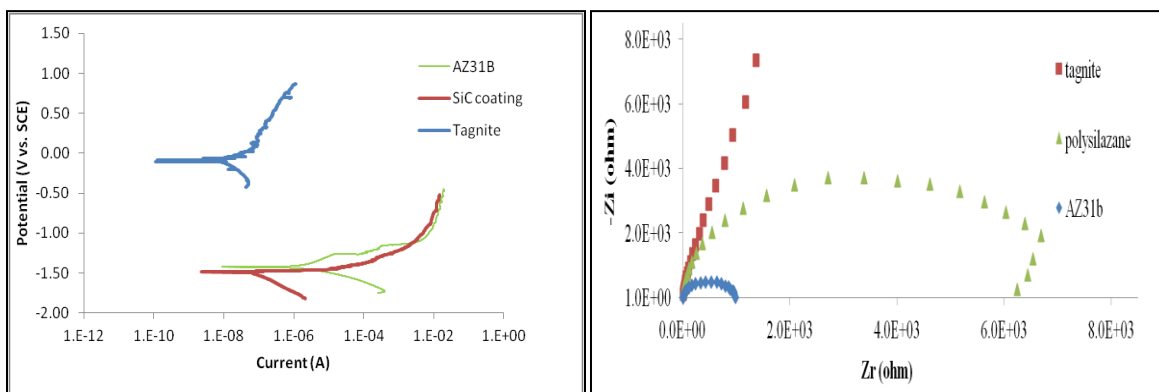
Figure 35. Influence of polysilazane coating on the electrochemical performance of AZ31B as determined by potentiodynamic polarization (left) and electrochemical impedance (right) spectroscopy measurements.

6.4   Magnesium in Personnel Protection

Given the combination of light weight and high specific stiffness, it is not surprising that Mg alloys have been or are being considered for a broad range of applications related to personnel protection. The first effort focused on the use of Mg as a potential means for improving the level of protection offered by helmets without significantly increasing their weight. Indeed, a flat plate test assembly plate demonstrated an approximate 30%−35% improvement in ballistic improvement over the current monolithic U.S. Army advanced combat helmet (ACH) baseline. It is particularly noteworthy that significant research was required to develop the optimal method for superforming the Mg alloy (WE43) sheet into the ACH helmet design with the desired specifications and minimal defects (see figure 36). Issues overcome during this effort ranged from the catastrophic failure of the sheet during forming to thickness variations between the crown and the edge of the helmet.

Figure 36. Representative helmet shapes made during series of superplastic forming trials, which resulted in a demonstrated ability to produce WE43 helmet shells with consistent quality.

Although the technique was developed to form helmets of consistent quality, improved protection could be achieved only if there is a strong bond at the Mg/ultrahigh weight molecular weight polyethylene (UHMWPE) interface. To achieve the strong bond necessary, atmospheric plasma treatment was evaluated as a potential means for modifying the surface of the UHMWPE backing layer. Testing of the resulting Mg/UHMWPE interface using lap shear testing indicated improved interfacial bond strength (see figure 37).

(a)   (b)
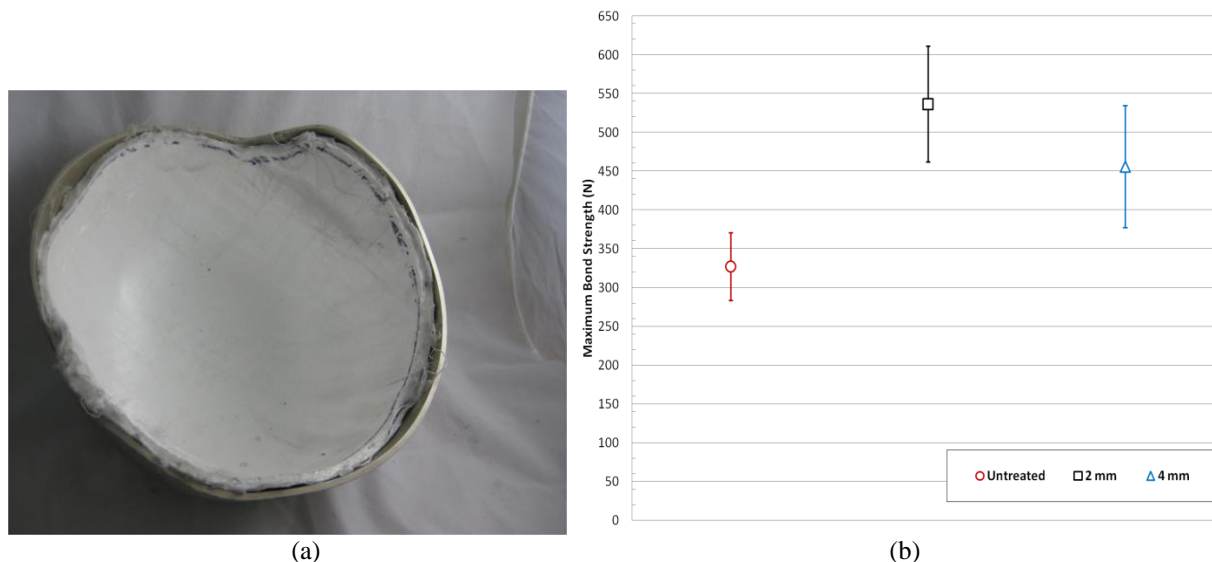
Figure 37. Photograph of WE43 helmet shell with attached UHMWPE backing layer (a) and test results
indicating the significant increase in bond strength between Mg and UHMWPE following
atmospheric plasma treatment (b).

Subsequent ballistic testing of flat panel test samples representing the intended helmet design
indicated that an approximate 5.7% increase in V_{50} could be obtained against 17-gr (1.1-g)
0.22-cal. fragment simulating projectile when a 2-mm WE43 strike face was used. However,
thicker WE43 layers actually resulted in a reduction in ballistic performance, as more weight of
the UHMWPE composite had to be removed to conserve the constant areal density. The results
were even more discouraging against the 7.62- $\times$ 39-mm threat, in that the best V_{50} was obtained
from the baseline UHMWPE panel (figure 38). The addition of a WE43 plate resulted in an
approximate 25% reduction in ballistic protection. Analysis of the rounds after testing indicated
that the projectile jackets were stripped, but the steel cores proceeded unscathed through the
plate. Based on this observation, it was decided that Mg alloys do not, on their own, have the
hardness required to blunt and/or deform the steel cores used in modern ballistic projectiles.
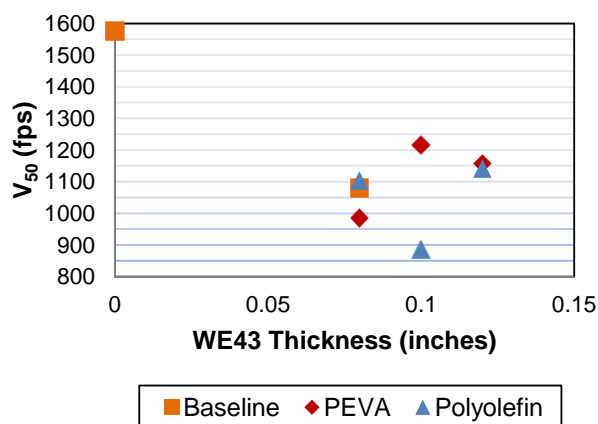
Figure 38. Ballistic performance of
WE43/UHMWPE test panel against
a 7.62- $\times$ 39-mm projectile.

38

Following the realization that Mg alloys were not suitable for helmet applications, consideration was given as to their potential for improving the performance of modern body armor. In addition to their light weight, Mg alloys also have a high specific stiffness and high damping capability. The high specific stiffness should enable a Mg backing plate placed behind the ceramic strike face to provide superior support over that provided by the UHMWPE during a ballistic impact event. The high damping capability of the Mg should result in a lower percentage of the tensile wave energy being reflected back into the ceramic strike face. Indeed, quick calculation indicates that only 22% of the tensile wave would be reflected back for a B_4C/WE43 panel compared with 73% for a B_4C/UHMWPE panel. It was theorized that this combination of properties would result in an improved multihit capacity for the ceramic strike face.

To test this hypothesis, two panel assemblies of equal areal density were constructed and tested against a representative ballistic threat. The first assembly tested was the conventional body armor layup (i.e., no Mg backing sheet). The second assembly incorporated a 0.076-in-thick WE43 backing layer behind the ceramic strike face. To remain areal density neutral, the thickness of the boron carbide (B_4C) ceramic strike face and UHMWPE backing layer were reduced (see table 6). Because of the limited facial area of the panels, only one shot per panel was possible. Five panels were tested for each configuration. Although it was not possible to determine a statistically accurate V_{50} figure because of the limited number of samples, the use of a 1×1 V_{50} (highest partial and lowest complete penetration) found that the assembly with the Mg backing layer had a normalized value of 0.98 compared with 1.0 for the conventional body armor assembly. This close agreement indicates that the panels offer a similar level of protection.

Table 6. Total areal density constant for both test panels at 7.01 psf.

Material	Baseline (no Mg layer) (in)	Mg Layer (in)
CoorsTek PAD B_4C tile	0.350	0.300
MENA WE43 sheet	—	0.076
Honeywell Spectra Shield II SR-3136 backing	0.450	0.415
Sikaflex-252	0.020	0.039

Representative photographs for both sets of test panels are shown in the following figures. The images in figure 39 are from the baseline (no Mg backing layer) samples and indicate the catastrophic damage in the ceramic strike face, including complete debonding of the ceramic from the UHMWPE backing layer. In addition, there is a significant amount of back-face deformation resulting from the ballistic impact. In comparison, images from the sample containing a WE43 Mg alloy backing layer (figure 40) indicate a lower level of damage to the ceramic strike face. The ceramic tile remains bonded to WE43 sheet and the first ply of backing. Furthermore, the WE43 plate spreads damage over larger area, resulting in a reduced amount of back-face deformation.

39

Figure 39. Baseline test panel; no Mg backing layer was used. Ballistic impact resulted in massive damage to tile, with the tile debonding from backing completely in most cases.
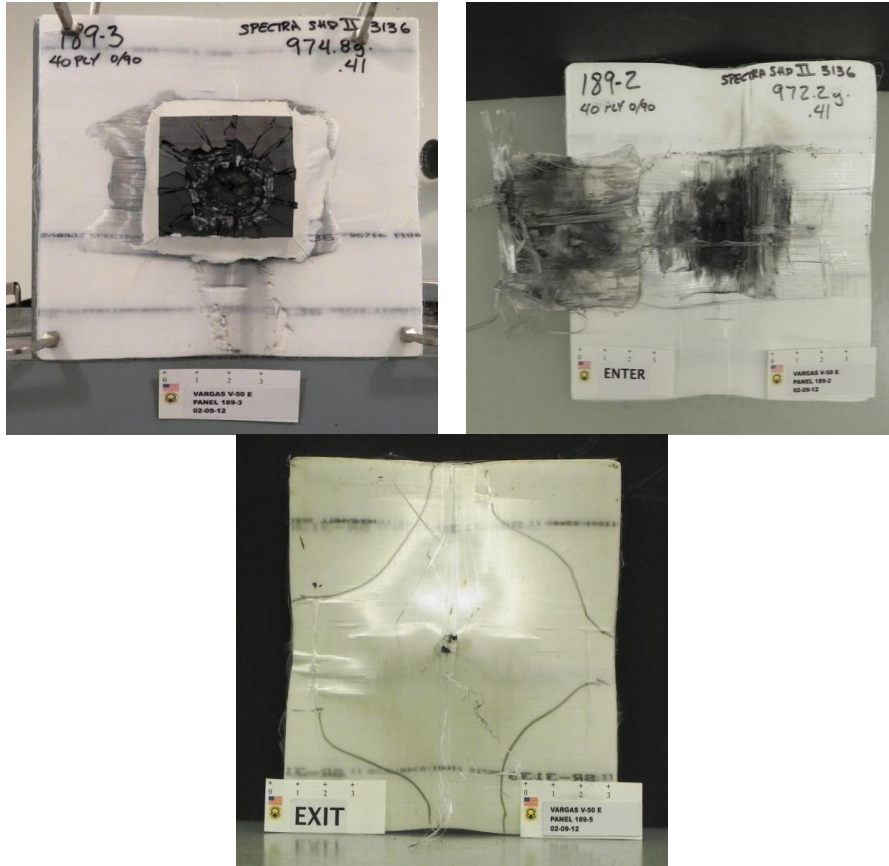
Figure 40. Images from the test panel with the WE43 Mg alloy backing layer. The amount of damage to the ceramic tile as well as back-face deformation is reduced relative to the baseline material shown in figure 36.

Figure 41 provides a comparison of the back-face deformation as a function of normalized projectile velocity for the two series. Although the current body armor design appears to outperform the new design that incorporates the Mg backing plate at the highest velocity levels, there is a clear trend of improving performance of the new design as the velocity is reduced. Provided this trend continues, the back-face deformation performance of the new design could very well be superior to the existing design at muzzle velocity and lower (approximately 0.746 normalized velocity). However, this supposition is still to be verified through ongoing testing.
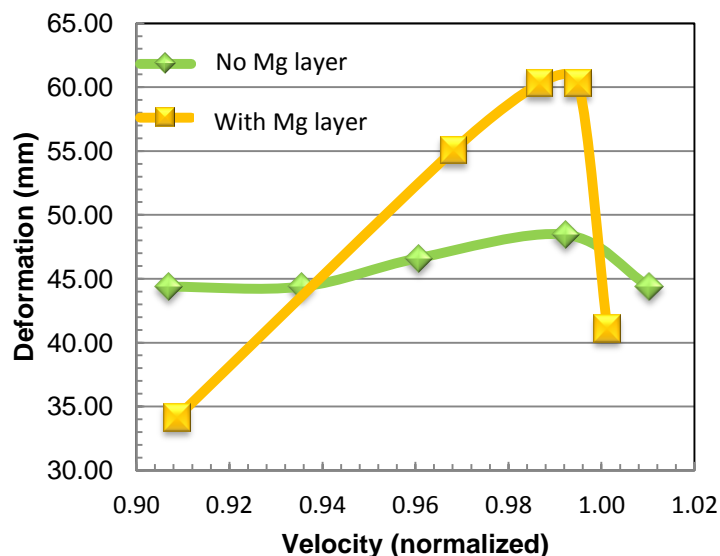
Figure 41. B$_4$C/WE43 panels show potential reduction in BFD at lower velocities. Muzzle velocity (approximately 0.746 normalized velocity) BFD should be superior if the trend continues downward.

7. Related External Work

In addition to the primary efforts discussed, there are a number of smaller efforts that serve to fill key research areas related to the development of Mg alloys. Often these efforts have minimal funding and represent a collaborative effort based on mutual interests and goals.

One such effort that has provided significant insight into the deformation mechanisms of Mg alloys is the computational analysis performed by the Center for Computational Materials Design at Pennsylvania State University (points of contact: Professors Zi-Kui Liu and Long-Qin Chen). Initial efforts focused on the use of phase field models to determine elastic constants and material response of polycrystalline Mg. Phase field models are highly useful for modeling Mg, as they can account for the influence of grain size and orientation on material response. For example, figure 42 provides a visual image of the viscoplastic deformation of Mg subjected to a 10% axisymmetric deformation along the z direction. Key observations are that the grain size does have an effect on the stress distributions, stress concentrations are present near grain boundaries, and no texture effects are readily observed.
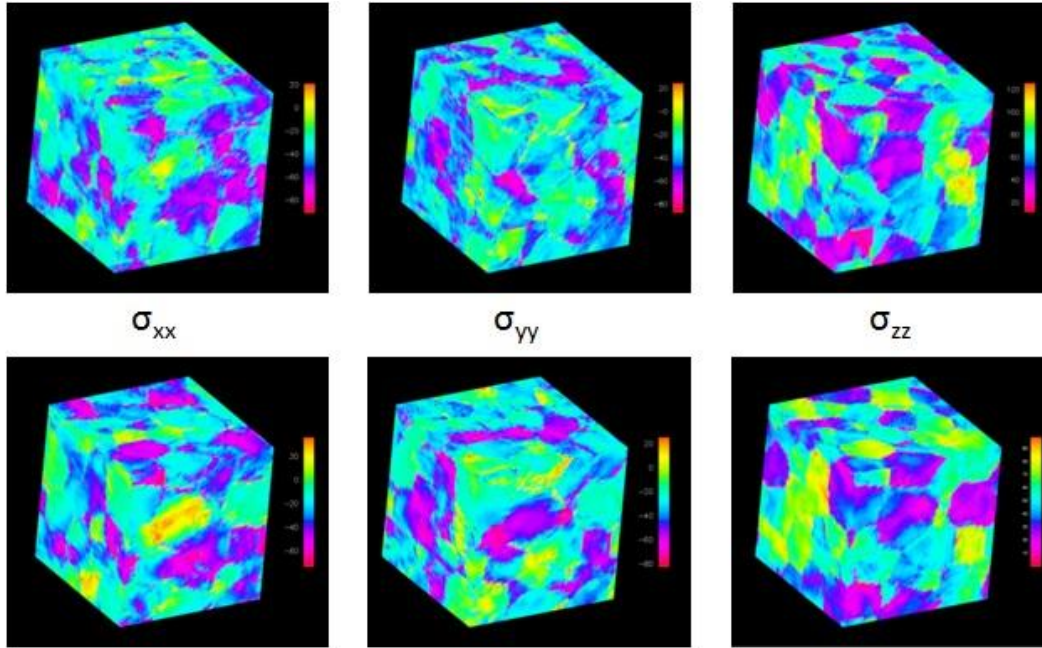
Figure 42. Deformation response of a Mg polycrystal subjected to deformation along the z axis.
The polycrystal in the top row has a grain size of 10.69 μ, and the one in the bottom
row has a grain size of 11.66 μ.

Figure 43 provides an additional example of the data that can be predicted using phase field
modeling. By drawing upon a typical polycrystal microstructure generated by phase field
simulations, the effective elastic constants and effective moduli (bulk, shear, Young's) of
polycrystalline Mg can be predicted. For the data shown in table 7, a system on the order of
$160 \times 160 \times 160$ μ (equivalent to approximately 10,000 gr) was used. Unfortunately, this
modeling approach did not progress further than the initial exploratory stage due to a lack of
funding.
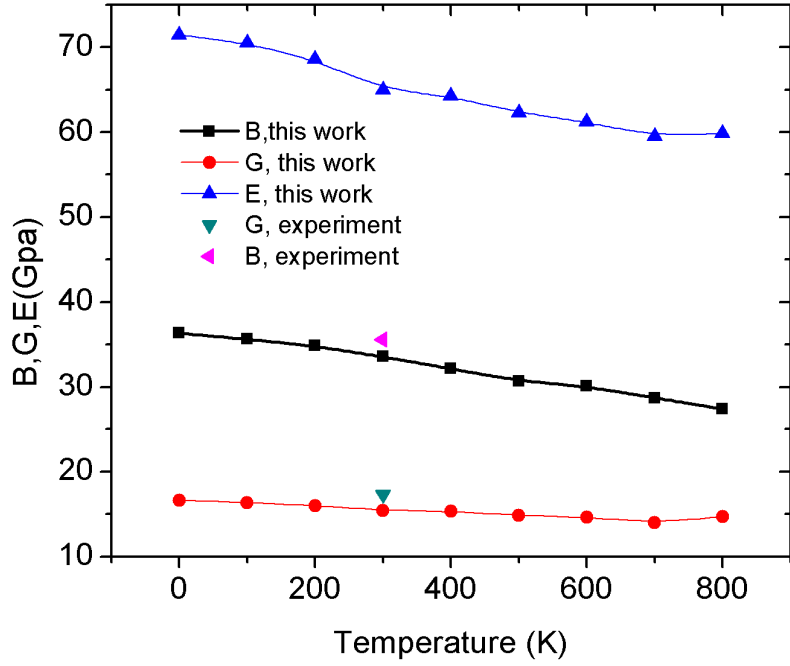
Figure 43. Calculated moduli values for polycrystalline Mg as
a function of temperature. Also shown are
experimental values for bulk and shear modulus.

Table 7. Comparison between predicted elastic constants for polycrystalline
Mg and those reported for a Mg alloy.

Structure	C_{11}	C_{12}	C_{13}	C_{33}	C_{44}
Polycrystal Mg (with sharp interfaces)	58.51	24.27	23.60	60.40	16.81
Mg-4.5Al-1Zn (literature data)	58.58	24.22	24.35	59.58	17.27

In addition, this collaboration has yielded a greater understanding into the influence of alloying
elements on the stacking fault energy (SFE) in Mg. Shown in figure 44 is the trend for both
intrinsic and extrinsic stacking fault energy for Mg-element binary alloy systems. The results
provide insight into why rare earth elements are so effective at improving properties of Mg, as
lower values of SFE promote deformation twinning and hence increased ductility.
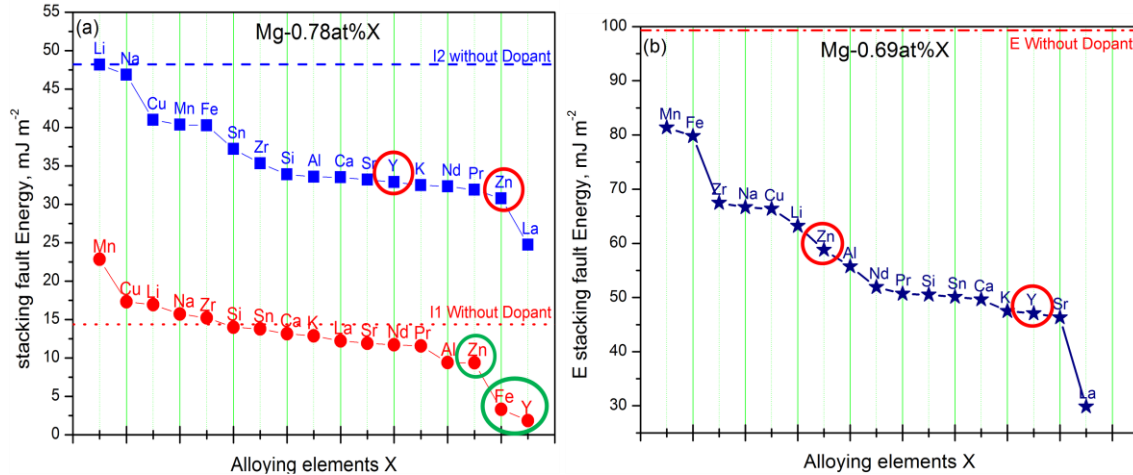
Figure 44. Influence of alloying addition on the SFE in binary Mg-X alloys of indicated composition. Curves in (a) are for intrinsic stacking faults, i.e., Growing (I1) and Deformation (I2), with the curve in (b) for extrinsic stacking faults.

Most recently, an effort has been made to model LPSO structures that are observed in select high-strength Mg alloys (figure 45). LPSO structures display lamellar morphology that comprise alternating layers of Mg (hcp) and an intermetallic (fcc) phase. These structures are classified by the period of the plane stacking ordering and whether they have hexagonal (H) or rhombohedral (R) periodicity. Typically, LPSO structures display 14H and 18R symmetry, with 18R transforming to 14H upon annealing. In this case, the models demonstrate that the formation of self-assembled atomic pillar nanoprecipitates in the LPSO structure may be a key strengthening mechanism.
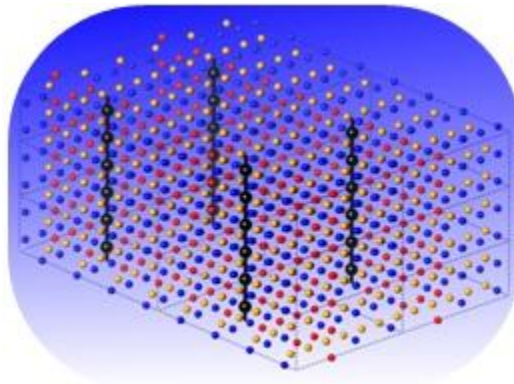
Figure 45. Atomistic representation of LPSO structure in unit cell.

In a recently started collaboration, we are working with Monash University of Melbourne, Australia, to evaluate the influence of atypical alloying elements (indium (In), lutetium (Lu), scandium (Sc), bismuth (Bi), etc.) on the mechanical and corrosion performance of AZ31B Mg alloy. After casting and extrusion, the mechanical and electrochemical performance of the 15 alloys was determined. Figure 46 relates yield strength to mass loss as well as relative toughness to corrosion current. As a result, they provide key insight into the elements that best improve the combined mechanical and electrochemical performance. By comparing the data points for the indicated alloying element to the AZ31B baseline point, it is clear that several elements improve the performance of AZ31. In particular, the following alloying elements were chosen for further study: arsenic, In, silver, strontium, and Sc. A second round of alloys will be cast and subsequently processed using ECAE in an attempt to achieve UFG materials for evaluation and testing.
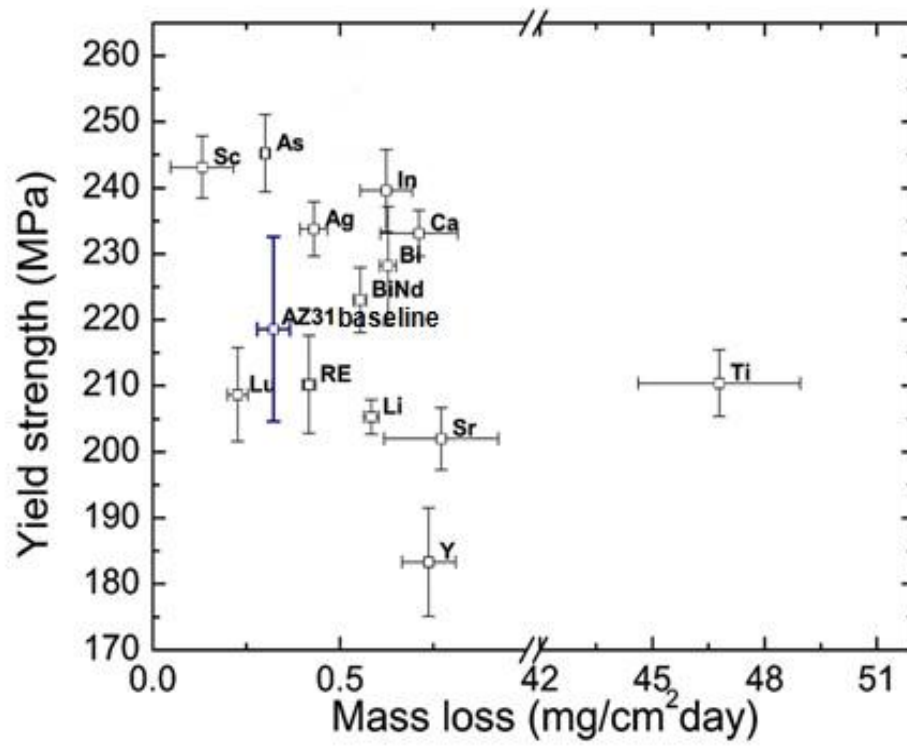
(a)
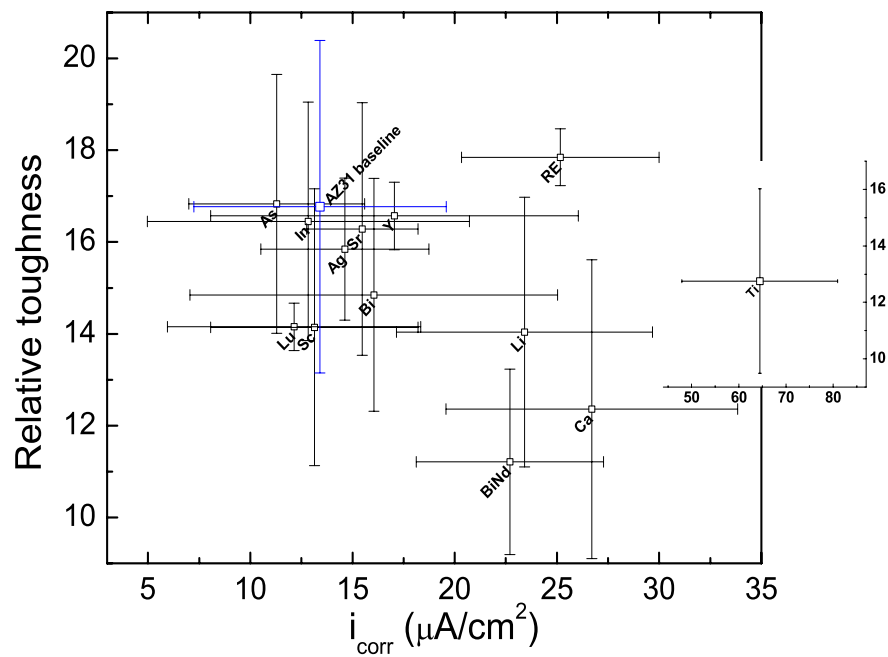
(b)

Figure 46. Relationship between (a) yield strength and mass loss and (b) relative toughness and corrosion current for each of the modified AZ31B alloys.

8. Summary

This report has reviewed the development, objectives, and accomplishments of the recently completed 5-year in-house ARL effort focused on ultrahigh-strength Mg alloys produced through the use of severe plastic deformation processing. Following an initial screening of various methods, ECAE was selected for continued study given its proven capability for microstructural refinement as well as its potential for up-scaling to industrially relevant dimensions. Initial efforts successfully established correlations between isothermal ECAE processing routes and microstructural refinement. Data collected during these experiments were used to verify computational models that were subsequently used to identify hybrid processing routes that incorporated progressive reductions in temperature. Consequently, these routes produced alloys with nanosized grains and random texture, thereby resulting in improved ductility and reduced anisotropy. Collectively, this developmental effort resulted in some of the highest tensile properties reported to date for AZ31B. In the last year of the program, the ECAE process development was expanded to plate geometries ($6 \times 6 \times 1/2$ in and $12 \times 12 \times 1$ in) as well as to additional alloy systems.

In addition, efforts during the same period also examined a number of related areas critical to the introduction of Mg alloys into U.S. Army systems. For example, the corrosion performance of numerous alloys was evaluated, thereby providing insight into the mechanisms that govern the long-term stability of these alloys in corrosion inducing environments. The potential of Mg in personnel protection was also investigated, with results indicating that, although not suited for helmet based applications, Mg appears to have potential for improving the performance of conventional body armor packages.

Finally, collaborative efforts with academic partners have explored the influence of alloying additions on the performance of Mg. Computational methods have identified those alloying elements that reduce SFE, thereby offering insight into potential alloys that might have improved ductility. A limited experimental study has identified a small number of alloying additions that show potential for improving both mechanical and electrochemical performance of AZ31B.

9. Future Directions

With the completion of the 5-year program and the beginning of the Materials in Extreme Dynamic Environments (MEDE) collaborative research alliance, there has been a natural shift in the focus of in-house Mg research. Through the MEDE program, the U.S. Army has partnered with a consortium of academic institutions, led by The Johns Hopkins University, to develop a

"materials by design" approach that relates material response across critical time and length scales to specific properties. After a survey of the general materials classes (metals, ceramics, polymers, and composites), a set of model materials—specifically Mg, boron carbide, ultrahigh-molecular-weight polyethylene fiber, and S-glass/epoxy composite—was chosen based on multiple factors, including the anticipated relevance of these materials to protection systems. To achieve this objective, research efforts are being developed in the following areas: advanced experimental techniques, modeling and simulation, synthesis and processing, materials characteristics and properties, and bridging the scales. In each area, a collaborative team made up of ARL and academic researchers has been established to address critical knowledge gaps that are limiting the suitability of that material to use in Army applications.

To align fundamental aspects of the in-house program with those of the MEDE program, research efforts have been split into 6.1 and 6.2 (basic and applied research, respectively) domains. The efforts in the 6.1 area primarily support MEDE-related efforts in the previously mentioned areas. Specifically, in-house 6.1 efforts are focused on verifying the accuracy of computational models to predict microstructural and texture evolution across various length scales, as well as the continued development of deformation processing methods to obtain UFG Mg alloys. Efforts in the 6.2 area focus on the ballistic and mechanical performance of UFG Mg alloys, with the goal of providing a well-grounded basis for the insertion of Mg alloys into an Army-relevant application. As a result, the primary focus is to compare the ballistic performance of ultrahigh-strength 12- × 12- × 1-in AZ31B plates with that of representative Al alloys and steels. In addition, an effort will evaluate the fatigue performance of UFG AZ31B, with an emphasis on determining how grain size and texture dictate material response. Knowledge gained from this effort will help to define the potential use of these alloys in struts, springs, or other components for lightening Army platforms. Finally, continued efforts in corrosion or, alternatively, potentially new starts in dynamic damping, multimaterial joining, or other areas are also being considered. These new areas are being determined through collaborative discussions with colleagues in ARL's Weapons and Materials Research Directorate, the Vehicle Technology Directorate, and the U.S. Army Tank Automotive Research, Development, and Engineering Center.

Taken as a whole, knowledge gained during this effort has appreciably advanced our understanding of Mg alloys, from the influence of alloying and processing to their performance under a broad range of test conditions and/or environments. As a result, the introduction of Mg alloys into Army systems is more likely today than when the project first started. This is certainly a worthwhile accomplishment, as Mg alloys represent a viable option for increasing performance while lowering weight in both personal and vehicle systems.

10. References

1. Mathaudhu, S. N.; Nyberg, E. A. Magnesium Alloys in U.S. Military Applications: Past, Current, and Future Solutions. In *Magnesium Technology 2010: Proceedings of a Symposium Sponsored by the Magnesium Committee of the Light Metals Division of TMS*, San Antonio, TX, 14–18 February 2010; The Minerals, Metals & Materials Society: Warrendale, PA, 2010, pp 27–34.

2. Brown, R. E. Magnesium in the 21st Century. *Advanced Materials and Processes* **2009,** *167* (1), 31–33.

3. *Magnesium Vision 2020: A North American Automotive Strategic Vision for Magnesium*, U.S. Automotive Materials Partnership, Southfield, MN, 2006.

4. Jones, T. L.; DeLorme, R. D.; Burkins, M. S.; Gooch, W. A. *Ballistic Evaluation of Magnesium Alloy AZ31B;* ARL-TR-4077; U.S. Army Research Laboratory: Aberdeen Proving Ground, MD, 2007.

5. Ma, E.; Ramesh; K. T.; Dowding, R.; McCauley, J. W. *International Magnesium Workshop;* ARL-SR-162; U.S. Army Research Laboratory: Aberdeen Proving Ground, MD, 2008.

6. Inoue, A.; Kawamura, Y.; Matsushita, M.; Hayashi, K.; Koike, J. Novel Hexagonal Structure and Ultrahigh Strength of Magnesium Solid Solution in the Mg-Zn-Y System. *Journal of Materials Research* **2001,** *16,* 1894–1900.

7. Agnew, S. R.; Horton, J. A.; Lillo, T. M.; Brown, D. W. Enhanced Ductility in Strongly Textured Magnesium Produced by Equal Channel Angular Processing. *Scripta. Materialia.* **2004,** *50,* 377–381.

8. Al-Maharbi, M.; Foley, D. C.; Hartwig, K. T.; Kecskes, L.; Mathaudhu, S. Microstructure and Properties of AZ31B Mg Alloy Processed by Equal Channel Angular Extrusion. In *Proceedings of the 8th International Conference on Magnesium Alloys and Their Applications,* Kainer, K.U., Ed. 2010; 26–29 October 2009, Weimar, Germany.

9. Al-Maharbi, M.; Foley, D.C.; Karaman, I.; Beyerlein, I.; Hartwig, K. T.; Kecskes, L.; Mathaudhu, S. Importance of Crystallographic Texture of AZ31B on Flow Stress Anisotropy and Tension-Compression Asymmetry. In *Magnesium Technolgoy 2010: Proceedings of a Symposium Sponsored by the Magnesium Committee of the Light Metals Division of TMS,* San Antonio, TX, 14–18 February 2010; The Minerals, Metals & Materials Society: Warrendale, PA, 2010.

10. Foley, D. C.; Al-Maharbi, M.; Hartwig, K. T.; Karaman, I.; Kecskes, L.; Mathaudhu, S. Mechanical Behavior of AZ31 Due to Texture and Microstructure. In *Magnesium Technology 2010: Proceedings of a Symposium Sponsored by the Magnesium Committee of the Light Metals Division of TMS,* San Antonio, TX, 14–18 February 2010; The Minerals, Metals & Materials Society: Warrendale, PA, 2010

11. Mathaudhu, S. N.; Kecskes, L. J. *Enhancement of Nanomaterials Processing Capabilities by the Addition of an ECAE Research Facility,* U.S. Army Research Laboratory, Aberdeen Proving Ground, MD, 2007.

12. Thompson, B.; Doherty, K. J.; Su, J.; Mishra, R. S. Nano-Sized Grain Refinement Using Friction Stir Processing. In *Friction Stir Welding and Processing VII,* Mishra, R. S., Mahoney, M. W.; Sato, Y.; Hovanski, Y.; Verma, R. The Minerals, Metals & Materials Society: Warrendale, PA, 2013, 9–19.

13. ASTM B 117, Standard Practice for Operating Salt Spray (Fog) Apparatus. *Annu. Book ASTM Stand.* **1973.**

14. Motz, G.; Kabelitz, T.; Ziegler, G. Polymeric and Ceramic-like SiCN Coatings for Protection of Light Metals Against Oxidation and Corrosion. *Key Engineering Materials* **2004,** *264–268,* 481–484.

INTENTIONALLY LEFT BLANK.

Appendix A. Personnel

Following is a list of the numerous U.S. Army Research Laboraoty personnel involved with the 5-year magnesium (Mg) development program.

Vincent Hammond: Program Manager since October 2010, Alloy Development

Suveen Mathaudhu: Program Manager, October 2008–2010

Laszlo Kecskes: Deformation Processing, Computational modeling

Brian Placzankis, Joseph Labukas: Corrosion studies

Shawn Walsh, Lionel Vargas: Magnesium in Personnel Protection

Kevin Doherty: Friction stir welding/processing

Tyrone Jones: Armor mechanism research and development of Mg alloy plates

Kris Darling: Magnesium powder processing

Kyu Cho: ManTech programs with Magnesium Elektron, NA

Matt Trexler, Blake Barnett, Marc Pepi: Cold spray of Mg powders

Appendix B. Publications

Publications related to the Mg program by ARL personnel or funded by ARL. Publications are arranged by year.

"Grain size engineering of BCC refractory metals: Top-down and bottom-up – Application to tungsten," LJ Kecskes, KC Cho, RJ Dowding, BE Schuster, RZ Valiev, & Q Wei, *Materials Science and Engineering A*, 467 (2007) 33-43.

"Dynamic behaviors of body-centered cubic metals with ultrafine grained and nanocrystalline microstructures," Q Wei, BE Schuster, SN Mathaudhu, KT Hartwig, LJ Kecskes, RJ Dowding, & KT Ramesh, *Materials Science and Engineering A*, 493 (2008) 58-64.

"Quasi-static and dynamic mechanical properties of commercial-purity tungsten processed by ECAE at low temperatures," Z Pan, YZ Guo, SN Mathaudhu, LJ Kecskes, KT Hartwig, & Q Wei, *Journal of Material Science*, 43 (2008) 7379-7384.

"Ultrafine and nanostructured refractory metals processed by SPD: Microstructure and mechanical properties," Q Wei, KT Ramesh, LJ Kecskes, SN Mathaudhu, & KT Hartwig, *Materials Science Forum*, 579 (2008) 75-90.

"Microstructures and recrystallization behavior of severely hot-deformed tungsten," SN Mathaudhu, AJ deRosset, KT Hartwig, & LJ Kecskes, *Materials Science and Engineering A*, 503 (2009) 28-31.

"Computational modeling of effects of alloying elements on elastic coefficients," ZK Liu, H Zhang, S Ganeshan, Y Wang, & SN Mathaudhu, *Scripta Materialia,* 63 (2010) 686-691.

"Corrosion comparisons among magnesium alloys of interest for DoD systems using laboratory based accelerated corrosion methods," BE Placzankis, CE Miller, SN Mathaudhu, & RD DeLorme, Paper # 10085, NACE Corrosion 2010 Conference and Expo.

"First-principles calculations of twin-boundary and stacking-fault energies in magnesium," Y Wang, LQ Chen, ZK Liu, & SN Mathaudhu, *Scripta Materialia*, 62 (2010) 646-649.

"Innovative Materials and Design for the Improvement of Warfighter Head Protection," LR Vargas & SM Walsh, 2010 Army Science Conference.

"Nanostructured materials by mechanical alloying: New results on property enhancement," CC Koch, RO Scattergood, KM Youssef, E Chan, & YT Zhu, *Journal of Materials Science*, 45 (2010) 4725-4732.

"Basal-plane stacking-fault energies of Mg: A first-principle study of Li- and Al- alloying effects," J Han, XM Su, ZH Jin, & YT Zhu, *Scripta Materialia,* 64 (2011) 693-696.

"Cationic doping of MgO surfaces to build corrosion protection in Mg alloys," H Kwak & S Chaudhuri, *J. Alloys Compounds*, 509 (2011) 8189-8198.

"Corrosion and ballistic analysis of new military grade magnesium alloys AMX602 and ZAXE1711 for armor applications," TL Jones, JP Labukas, BE Placzankis, & K Kondoh, Paper #20369, DoD Corrosion Conference 2011.

"Deformation twinning in a nanocrystalline HCP Mg alloy," XL Wu, KM Youssef, CC Koch, SN Mathaudhu, LJ Kecskes, & YT Zhu, *Scripta Materialia*, 64 (2011) 213-216.

"Dislocation-twin interactions in nanocrystalline FCC metals," YT Zhu, XL Wi, XZ Liao, J Narayan, LJ Kecskes, & SN Mathaudhu, *Acta Materialia*, 59 (2011) 812-821.

"Grain refinement vs. crystallographic texture: Mechanical anisotropy in AZ31B magnesium alloy processed via a hybrid ECAE route," DC Foley, M Al-Maharbi, KT Hartwig, I Karaman, LJ Kecskes, & SN Mathaudhu, *Scripta Materialia*, 64 (2011) 193-196.

"High hardness in a nanocrystalline Mg97Y2Zn1 alloy," KM Youssef, YB Wang, XZ Liao, SN Mathaudhu, LJ Kecskes, YT Zhu, & CC Koch, *Materials Science and Engineering A,* 528 (2011) 7494-7499.

"High strength, nano-structured Mg-Al-Zn alloy," B Zheng, O Ertorer, Y Li, Y Zhou, SN Mathaudhu, CYA Tsao, EJ Lavernia, *Materials Science and Engineering A*, 528 (2011) 2180-2191.

"Microstructure, crystallographic texture, and plastic anisotropy evolution in a Mg alloy during equal channel angular extrusion processing," M Al-Maharbi, I Karaman, IJ Beyerlein, D Foley, KT Hartwig, LJ Kecskes, & SN Mathaudhu, *Materials Science and Engineering A,* 528 (2011) 7616-7627.

"Control of the interfacial properties of ultrahigh molecular weight polyethylene / magnesium hybrid composites through use of atmospheric plasma treatment," LR Vargas, SM Walsh & DD Pappas, *Polymer Composites*, 33 (2012) 207-214.

"Effect of grain size on prismatic slip in Mg-3Al-1Zn alloy," SM Razavi, DC Foley, I Karaman, KT Hartwig, O Duygulu, LJ Kecskes, SN Mathaudhu, & VH Hammond, *Scripta Materialia*, 67 (2012) 439-442.

"Effective elastic properties of polycrystals based on phase-field description," G Sheng, S Bhattacharyya, H Zhang, K Chang, SL Shang, SN Mathaudhu, ZK Liu, & LQ Chen, *Materials Science & Engineering A*, 554 (2012) 67-71.

"Electron localization morphology of the stacking faults in Mg: A first-principles study," WY Wang, SL Shang, Y Wang, KA Darling, SN Mathaudhu, XD Hui, & ZK Liu, *Chemical Physics Letters*, 551 (2012) 121-125.

"Microstructural evolution and mechanical properties of niobium processed by equal channel angular extrusion up to 24 passes," Z Pan, F Xu, SN Mathaudhu, LJ Kecskes, WH Yin, XY Zhang, KT Hartwig, & Q Wei, *Acta Materialia*, 60 (2012) 2310-2323.

NO. OF
COPIES ORGANIZATION

  1   DEFENSE TECHNICAL
(PDF) INFORMATION CTR
       DTIC OCA

  1   DIRECTOR
(PDF) US ARMY RESEARCH LAB
       IMAL HRA

  1   DIRECTOR
(PDF) US ARMY RESEARCH LAB
       RDRL CIO LL

  1   GOVT PRINTG OFC
(PDF) A MALHOTRA

  1   RDRL WMM F
(PDF)   V HAMMOND